CLM - R 7

CLM - R 7

United Kingdom Atomic Energy Authority

RESEARCH GROUP

Report

TOROIDAL DISCHARGE CONFIGURATIONS OBTAINED FROM MAGNETIC PROBE MEASUREMENTS

E. A. WITALIS

Culham Laboratory,

Culham, Abingdon, Berks.

1961

Available from H.M. Stationery Office

SEVEN SHILLINGS NET

U.D.C.
621.039.667.6.026

CLM - R7

TOROIDAL DISCHARGE CONFIGURATIONS OBTAINED FROM MAGNETIC PROBE MEASUREMENTS

by

E.A. Witalis*

ABSTRACT

Low pressure argon discharges in the Mk IV torus have been studied by magnetic probe technique during the early part of the discharge when the results so given are reproducible. A method of analysis is presented here by which the experimental results may be compared with those predicted by two theoretical models. It is shown that neither model is wholly satisfactory in this case. Several types of discharge are found, one of which corresponds to a "rigid" behaviour of the current helix which occurs just before the onset of irreproducibility of the magnetic probe signals.

U.K.A.E.A. Research Group,
Culham Laboratory,
Culham, Nr. Abingdon,
Berks.

July, 1961

HL61/3480 (C.18)
/PMF

*Present Address: Division of Electronics, Royal Institute of Technology, Stockholm, Sweden.

CONTENTS

		Page
Introduction		1
1.	Experiments and analysing methods.	2
	1a. The experimental apparatus	2
	1b. The discharge types	2
	1c. Field component curves	2
	1d. The m- and n- curves	4
	1e. Other experimental curves	6
2.	Theory	7
	2a. The "fluid" model	7
	2b. The Bessel function model	10
	2c. The use of configuration models	12
	2d. The axial flux conservation	13
	2e. The channel surface region	14
3.	The experimental results and their interpretation	15
	3a. The onset of large instabilities. Experimental facts.	15
	3b. The onset of large instabilities. Explanation	16
	3c. Discharge A.	17
	3d. Discharge B.	18
	3e. Discharge C.	19
4.	Summary and conclusions	20
	Acknowledgements	20
	References	21

TABLE

Table	
I	3

ILLUSTRATIONS

Fig. 1 The "fluid" model for ε = 0, 0.5 and 1.

Fig. 2 The Bessel function model for ε = 0, 0.33 and 1.

Fig. 3 m - and n - curves from the theoretical models.

Fig. 4 Oscillogram. Discharge A. B_z and I_z, r = - 3 cm.

Fig. 5 " Discharge B. B_z and I_z, r = 0.

Fig. 6 " Discharge C. B_ϕ and I_z, r = 2 cm.

Fig. 7 Field components for discharge A.

Fig. 8 m - and n - curves for configuration AI.

Fig. 9 " " " AII.

Fig. 10 " " " AIII.

Fig. 11 Discharge A. B_{zo}, ΔB_z and B_{min} as functions of I_z.

Fig. 12 " m(0) and $\bar{n}$ as functions of I_z.

Fig. 13 Field components for discharge B.

Fig. 14 m - and n- curves for configuration BI.

Fig. 15 " " " BII.

Fig. 16 " " " BIII.

Fig. 17 Discharge B. B_{zo}, ΔB_z and B_{min} as functions of I_z.

Fig. 18 Field components for discharge C.

Fig. 19 m- and n- curves for configuration CI.

Fig. 20 " " " CII.

Fig. 21 " " " CIII.

Fig. 22 " " " DIII.

INTRODUCTION

In the course of a general study of toroidal magnetic field configurations carried out by Lees and Rusbridge[1] it was found that under certain conditions the measured parameters disagreed with the general pattern. It was therefore considered important from the point of view of establishing and extending the usefulness of the treatment described in reference (1) to investigate these 'anomalous' cases by a detailed study of magnetic field configurations.

The purpose of the present report is to describe the experimental investigation of one of these cases, namely the early stages of a low pressure argon discharge in the Mk IV torus. In this case the experimental results are reproducible to a high order and consequently complete magnetic configurations and their time variations can be plotted without recourse to a statistical treatment. Two theoretical models, one of which was used in the previous work are given, although neither is sufficient to explain the complex behaviour of the discharge. This report therefore confines itself mainly to presenting some representative experimental analyses and tries to give theoretical explanations only where these are obvious.

1. EXPERIMENTS AND ANALYSING METHODS

1a. The experimental apparatus

The measurements have been made at an initial Argon gas pressure of 1μ in the discharge of the Mk IV torus which is of generally the same design as ZETA. The torus has 15.5 cm bore radius and an aspect ratio of 1:4. The measurements were made according to the well established magnetic search coil technique[2].

The Mark IV torus, the integrators, the search coils and the recording instruments have already been thoroughly described in a previous paper[3].

The magnetic search coil was air cooled and inserted in a glass tube of 2 cm diameter. This tube coincided with the horizontal torus cross section diameter at the window block.

1b. The discharge types

A "discharge type" was investigated by measuring the axial and tangential magnetic field components at intervals of 1 cm along the torus cross section diameter. If no such other variable as initial gas pressure, initial magnetic field etc., was changed, the reproducibility was very good up to a time when large instabilities suddenly began to appear. The measurements were made in such a rapid succession (≈ 2 sec.) that the afterglow from the oscillogram traces of the preceding discharge can be seen on any oscillogram. Three measurements were made at each point. These facts provide a simple check of possible sudden changes. No unexpected irreproducibilities have been found in this way. Slow uncontrolled variations of the discharge conditions cannot be discovered by this method but they would be seen by a comparison of the photographs of the main current traces. Only in one case did a discharge type investigation fail to satisfy this test and have to be discarded. The reason for the current variation has been found to be purely instrumental.

Different discharge types have been obtained only by changing the applied electric field strength and hence the main discharge current I_z and, in one case, by increasing the initial static magnetic field B_i from 50 to 100 gauss.

Three representative discharge types have been selected to be presented here. They will be referred to as A, B and C. A Roman number I, II or III, added to the capital letter, will indicate one of three investigated configurations for each discharge type. See Table I.

Earlier investigations of toroidal discharges have shown that they can, to some extent, be characterised by a pinch parameter θ defined by

$$\theta = \frac{\mu_o I_z}{2\pi a B_i}$$

where a is the torus bore radius. θ is thus the ratio of the tangential magnetic field strength at the torus inside wall and the initial axial field strength B_i. The θ -values in the actual cases are given in Table I.

TABLE I

Discharge	B_i (gauss)	I_{zp} (kA)*	θ_p*	N:o	t(μs)	I_z (kA)	θ	B_{zo} (gauss)
A	50	9.69	2.50	I	70	5.13	1.32	131
				II	90	6.53	1.69	174
				III	110	7.54	1.95	194
B	100	9.75	1.26	I	80	4.57	0.59	124
				II	120	6.86	0.89	151
				III	160	8.33	1.08	183
C	50	11.83	3.05	I	50	6.47	1.67	190
				II	60	7.35	1.89	216
				III	70	8.16	2.11	238

*The index p refers to peak current

1c. Field component curves

The complete magnetic field configuration has been plotted and analysed for three times during the period of each discharge type. The method of analysis will be described in the next sections.

The first configuration is always given for the earliest possible time permitted by the accuracy of the oscillograms and the last is always just before or at the onset of large irreproducible instabilities.

As a single field curve contains 34 experimental points, and each point is the average of three separate measurements, one complete investigation of a configuration is based upon 2 x 3 x 34 measurements and as many actual discharges. The right hand side of a configuration curve always refers to the torus inside. The toroidal geometry deviation is mainly seen as a relative

increase of the tangential B_ϕ - field there.

Except in the cases where the deviation due to toroidal geometry is critical, all the analysis of the experimental results and the theoretical calculations and models are obtained from the usual cylindrical geometry (r, ϕ, z) around a magnetic centre line defined by $B_\phi = 0$. However in order to show possible wriggling of the plasma channel all the experimental configuration curves are given in a co-ordinate system which is fixed relative to the torus.

1d. The m - and n - curves

The pressure balance relation

$$-\frac{dp}{dr} = i_z B_\phi - i_\phi B_z \qquad \ldots\ldots 1.$$

connects the macroscopic mechanical and electrical properties of a cylindrically symmetrical plasma. It is possible to obtain a simple physical interpretation of this equation by rewriting it as

$$-\frac{dp}{dr} = \frac{r}{R} i_z B_z (m - n) \qquad \ldots\ldots 2.$$

where

$$m = m(r) = R \frac{B\phi}{rB_z}$$

is the number of turns which the helical magnetic lines of force make around the centre line. m refers to the length $2\pi R$ of that centre line, i.e. neglecting toroidal deviations, R is the torus major radius.

This concept of the turn number m can be visualised by considering the cylindrical surface r = const. cut up so as to form a rectangle of the dimensions $2\pi R \times 2\pi r$ with the magnetic lines of force as straight lines upon it and inclined the angle arc tg $\frac{B\phi}{B_z}$ to the side of the length $2\pi R$.

In the same way

$$n = n(r) = R \frac{i_\phi}{ri_z}$$

is the corresponding quantity for the helical current paths.

Neither m nor n is assumed to be an integral number. For m, such a case implies that each line of force closes upon itself when returning to a starting

tube cross section after traversing its helical path one turn along the torus tube. This fact can be put in this way: an integral m corresponds to the same integral multiple of the Kruskal limit (m = 1).

Integral n may have important consequences. Such conditions will later be discussed in more detail.

According to the above expressions, m(r) and n(r) become indefinite for r = 0 as i_ϕ (0) = $B_\phi(0)$ = 0. However, in that case, m and n must be regarded as the limit values obtained by r $\longrightarrow$ 0. They are denoted m_o and n_o. (The index o will generally refer to quantities at r = 0, except in obvious cases like μ_o and the Bessel function J_o.)

It should be noted that n_o does not necessarily equal m_o. This may seem odd as there are no pressure gradients at r = 0 for symmetry reasons. Accordingly the deduced helix systems of current and magnetic field should coincide there. This seeming contradiction is only due to the limiting process, as can be seen, for instance, by inserting a pressure distribution of Bennett type, $p = p_o (1 + Cr^2)^{-2}$, in eq. 2 and obtaining $m_o \neq n_o$ but $\left(\frac{dp}{dr}\right)_o = 0$.

The inward pinching force is, according to eq. 2, proportional to the difference m - n which may be expected to be small compared with m or n. Therefore, highest possible accuracy has been required for the measurements giving m(r) and n(r).

The function m(r) has been calculated directly point by point, by using the experimentally obtained values of the magnetic configuration.

From the equations

$$i_\phi = -\frac{1}{\mu_o}\frac{d}{dr}(B_z) \qquad \text{..... 3.}$$

$$i_z = \frac{1}{\mu_o r}\frac{d}{dr}(rB_\phi)$$

the current turn number n(r) can be expressed as

$$n(r) = R\frac{i_\phi}{ri_z} = -R\frac{\frac{d}{dr}(B_z)}{\frac{d}{dr}(rB_\phi)} \qquad \text{..... 4.}$$

$n(r)$ has been calculated as the ratio of the quantities $-\delta(RB_z)$ and $\delta(rB_\phi)$ where δ indicates the difference between experimental magnetic field strength values for points situated 2 cms apart. Thus $n(r)$ is not obtained from the slopes of "smoothed out" magnetic field curves and this fact causes a fairly large "spread" for adjacent points of the $n(r)$- curve.

1e. Other experimental curves

An average value of n, referring to the whole plasma channel, is obtained as

$$\bar{n} = \frac{I_\phi}{I_z} = \frac{1}{I_z} \cdot \frac{2\pi R}{\mu_o} (B_{zo} - B_{min}) = \frac{2\pi R}{\mu_o I_z} \Delta B_z$$

where

$$I_z = \int_0^a i_z \, 2\pi r \, dr,$$ where a is the torus bore radius.

B_{min} is the average value of the two measured minima of the B_z-field. The plasma channel is thus defined here as the region inside the z-field minimum. The average value for B_{min} is taken in order to correct for the field deviations due to the toroidal geometry.

I_ϕ is the total plasma channel current in ϕ-direction, i.e. perpendicular to the applied electric field. I_ϕ is directly proportional to and calculated from $B_{zo} - B_{min} = \Delta B_z$.

As I_z is measured by a Rogowski coil outside the torus tube, $\bar{n}$ is a true average only if the z-current going in the annular space between the z-field minimum and the torus wall can be neglected. Such a current will make $\bar{n}$ smaller than the average of the n-curve points.

B_{zo}, ΔB_z and the two minimum values of B_z have been plotted as functions of I_z. A figure beside an experimental point indicates the time after the discharge start.

Three photographs of oscillograms give the total discharge current I_z as function of time (bottom trace) for the three presented discharge types. The top traces are the integrated probe signals in some cases of special interest, to be discussed later.

2. THEORY

Two theoretical discharge configurations will be given and the use of such model configurations is then discussed. Some other theoretical concepts for the experiment interpretation will be found in the last sections.

2a. The "fluid" model

This configuration model is deduced from the following two assumptions:

Firstly, n is independent of r, i.e. the drift motion of the charged particles resembles a shearfree fluid motion. Regarding the macroscopic plasma current as a comparatively slow drift motion superimposed upon a faster thermal motion, this assumption seems to be reasonable and it will be shown that it is confirmed by experimental n-curves in some cases.

Secondly the pressure dependence in R is assumed to be

$$p = p_o \left(1 + \left(\frac{r}{r_c}\right)^2\right)^{-2}$$

A density distribution of this Bennett type is known to be a good approximation for low and medium current discharges with stabilizing magnetic field. The radius r_c will be put equal to the characteristic length $\frac{R}{n}$ of the discharge, an assumption leading to a gas pressure nearly proportional to the magnetic pressure $\frac{B_z^2}{2\mu_o}$ of the pinched z-field.

It should be noted that the original Bennett distribution with

$$r_c^2 = \frac{8\, p_o}{\mu_o\, i_{zo}^2}$$

is not assumed here since it applies to conditions quite different from those investigated and further, that any reasonable pressure distribution could be used together with the fundamental first assumption. The distribution assumed here can be expected to be a good approximation for low θ-values and it will not lead to combersome mathematical expressions.

The first assumption, n independent of r, makes eqn. 4 readily integrable.

$$B_z = B_{zo} - B_\phi \frac{nr}{R} = B_{zo} - B_\phi \tan \psi$$

where ψ is the angle between current direction and ϕ-direction.

The current components can be written

$$i_\phi = i_{zo}\, f(r) \sin \psi$$

$$i_z = i_{zo}\, f(r) \cos \psi$$

where $f(r)$ is the dimensionless ($f(0) = 1$) magnitude of the current density in the drift motion direction. The current density direction is thus determined by the fundamental first assumption and the function $f(r)$ now has to be determined.

Inserting the above three equations in the pressure balance relation, eqn. 1, gives

$$-\frac{dp}{dr} = i_{zo}\, f(r)\, B_\phi \cos \psi - i_{zo}\, f(r)\, (B_{zo} - B_\phi \tan \psi) \sin \psi$$

writing

$$p(r) = p_o\, g(r), \quad g(0) = 1$$

$$B_\phi = \frac{\mu_o}{r} \int_o^r i_z\, r\, dr = \frac{\mu_o}{r} \int_o^r i_{zo}\, f(r) \cos \psi\, r\, dr$$

and using the expressions for $\sin \psi$ and $\cos \psi$ when $\tan \psi = \frac{nr}{R}$, the pressure balance relation gives an integral equation for $f(r)$

$$-\frac{P_o}{i_{zo}} \frac{dg}{dr} \left(1 + \left\{\frac{nr}{R}\right\}^2\right)^{\frac{1}{2}} = f(r) \left[\left(1 + \left\{\frac{nr}{R}\right\}^2\right) \frac{\mu_o}{r} \int_o^r f(r) i_{zo} \left(1 + \left\{\frac{nr}{R}\right\}^2\right)^{-\frac{1}{2}} r\, dr - B_{zo} \frac{nr}{R} \right]$$

Introducing the dimensionless quantities β and ε

$$\beta = \frac{i_{zo}^*}{i_{zo}} = \frac{2\, B_{zo}\, n}{\mu_o\, i_{zo}\, R}$$

where i_{zo}^* is the centre current density in the special case $p_o = 0$, and

$$\varepsilon = \frac{2\mu_o\, p_o}{B_{zo}^2}$$

is the ratio of centre gas pressure to corresponding magnetic pressure and changing variables

$$\frac{nr}{R} = x$$

$$f(x^2)\ (1 + x^2)^{-\frac{1}{2}} = Y\ (x^2)$$

the integral equation turns out

$$-\left(\frac{\beta}{2}\right)^2 \varepsilon\ \frac{dg}{dx}\ x\ (1 + x^2)^{-1} = Y(x^2) \left[\int_0^{x^2} Y(t)\ dt - \beta\ x^2\ (1 + x^2)^{-1} \right]$$

By inserting the assumed pressure distribution

$$g\ (x^2) = (1 + x^2)^{-2}$$

the integral equation can be solved approximately

$$y(x^2) = \beta\ (1 + x^2)^{-2} + \varepsilon\beta\ (1 - x^2)\ (1 + x^2)^{-3}$$

Hence the current components are

$$i_z = i_{zo}^* \left[(1 + x^2)^{-2} + \varepsilon\ (1 - x^2)\ (1 + x^2)^{-3} \right]$$

$$i_\phi = i_z\ x$$

Using the eqns. 3, these two equations are integrated to give the magnetic field components

$$B_z = B_{zo}\ (1 + x^2)^{-1} \left[1 - \varepsilon\ x^2\ (1 + x^2)^{-1} \right]$$

$$B_\phi = B_{zo}\ x\ (1 + x^2)^{-1} \left[1 + \varepsilon\ (1 + x^2)^{-1} \right]$$

$\frac{B_z}{B_{zo}}$ and $\frac{B_\phi}{B_{zo}}$ are shown graphically in Fig. 1 for the three cases $\varepsilon = 0,\ 0.5$ and 1.

The field components are inserted in the expression for the magnetic turn number m.

$$m = R\ \frac{B_\phi}{rB_z} = n\ (1 + \varepsilon + x^2)\ (1 + x^2\ (1 - \varepsilon))^{-1} \approx n\ (1 + \varepsilon)$$

This model thus makes the difference between the n - and m - curves proportional to the center gas pressure.

As would be expected, the magnetically shearfree and forcefree configuration defined by

$$\frac{i_\phi}{i_z} = \frac{B_\phi}{B_z} = \frac{nr}{R}, \quad n \text{ independent of } r$$

is obtained by putting po = ε = 0 in all above equations. In all experimental cases the parameter ε is considerably smaller than unity and therefore the gas pressure influence is seen as small terms added to the equations of the force free model (the curves ε = 0 in Fig. 1). These terms depend only upon the chosen gas pressure distribution g(x) and the turn number n. Thus, if the fundamental assumption n = const. has experimentally been found valid, it is possible to obtain the unique magnetic field and current configuration which corresponds to a given gas pressure distribution and vice versa.

2b. The Bessel function model

The Bessel function model

$$B_\phi = A_\phi \, J_1 (\alpha r)$$
$$B_z = A_z \, J_o (\alpha r)$$

has been used as the basis for an earlier extensive investigation of toroidal magnetic configurations[1]. One reason for choosing Bessel functions was that they can be fitted to agree fairly well with experimental configurations.

The above Bessel functions of zero and first order with $A_\phi = A_z$ are obtained as the solution of the equation, (4)

$$\mu_o \underline{i} = \text{curl } \underline{B} = \alpha \underline{B}, \quad \alpha \text{ independent of } r,$$

for cylindrically symmetrical geometry, i.e. $\underline{B} = (0, B_\phi (r), B_z(r))$. As seen from the vector equation its solution must describe a force free configuration where the current density and the magnetic field strength are everywhere proportional.

In the earlier investigation the pressure influence was accounted for by putting $A_\phi > A_z$. Inserting the field components in the equations 3, the current components were obtained:

$$i_z = \frac{\alpha A_\phi}{\mu_o} \, J_o (\alpha r)$$

$$i_\phi = \frac{\alpha A_z}{\mu_o} \, J_o (\alpha r)$$

From the definition of m (0) = m_o and n(0) = n_o

$$m_o = \lim_{r \to 0} R \left(\frac{B_\phi}{r B_z} \right) = R \frac{\alpha A_\phi}{2 A_z}$$

$$n_o = \lim_{r \to 0} R \left(\frac{i_\phi}{r i_z} \right) = R \frac{\alpha A_z}{2 A_\phi}$$

Thus the constant α is here identified as

$$\alpha = 2 \frac{(m_o n_o)^{\frac{1}{2}}}{R}$$

and the two constants A_ϕ and A_z can be written

$$A_\phi = A (m_o)^{\frac{1}{2}}$$

$$A_z = A (n_o)^{\frac{1}{2}}, \text{ where A is constant.}$$

Substitution in the pressure balance, equation 1, and integration from 0 to r gives

$$p(r) = p_o + \frac{A^2 (m_o - n_o)}{2 \mu_o} \left[J_o^2 (\alpha r) - J_o^2 (0) \right]$$

Following the earlier deduction it is here assumed that p = 0 where $B_z = 0$, i.e. where $\alpha r_o = 2{:}405$ which is the first root of the equation $J_o (\alpha r) = 0$.

This condition inserted in the pressure equation above gives

$$p_o = \frac{A^2 (m_o - n_o)}{2 \mu_o}$$

and thus

$$\varepsilon = \frac{2 \mu_o p_o}{B_{zo}^2} = \frac{m_o}{n_o} - 1, \quad m_o = (1 + \varepsilon) n_o$$

This Bessel function model can now be compared with the previously deduced "fluid" model, where n is constant. Therefore the component equations of the Bessel function model are written so that they contain the quantities n_o and ε.

$$B_z = A (n_o)^{\frac{1}{2}} J_o (\alpha r) = B_{zo} J_o (\alpha r)$$

$$B_\phi = A (n_o (1 + \varepsilon))^{\frac{1}{2}} J_1 (\alpha r) = B_{zo} (1 + \varepsilon)^{\frac{1}{2}} J_1 (\alpha r)$$

$$\alpha = \frac{2}{R} n_o (1 + \varepsilon)^{\frac{1}{2}}$$

The graphs of $\frac{B_z}{B_{zo}}$, $\frac{B_\phi}{B_{zo}}$ have been drawn in fig. 2 with $\frac{n_o r}{R}$ as the dependent variable for the three cases $\varepsilon = 0$, 0.33 and 1. It can be noted that only the region for which $B_z > 0$ can give a good approximation of the experimental curves and further that variations of the pressure parameter ε have the same influence upon the configuration as in the "fluid" model case.

2c. The use of configuration models

Experimental results can be interpreted by comparisons with configuration models but it will be shown that there is much required both from the experiments and the models. Thus the model should describe a unique configuration deduced from reasonable physical assumptions and the experiments must be accurate enough to distinguish between various possible models.

The experimental magnetic configurations have been compared with the two given models and it has been found that neither is in perfect agreement. The curves often seem to be some sort of mean between the two models. However this way of direct comparing field components is less satisfactory for two reasons. Firstly, the investigated cases only apply to the central region where the models are not very different (cf. Figs. 1 and 2) and secondly, very little information is given about the physical reasons for the discrepancies. A better way is to compare the experimental and theoretical m- and n-curves, since some physical information is then obtained and model differences are enlarged.

Thus for the Bessel function model

$$m(r) = R\,\frac{B_\phi}{rB_z} = R\left(\frac{m_o}{n_o}\right)^{\frac{1}{2}}\frac{J_1(a\,r)}{r\,J_o(a\,r)} = R\,(1+\varepsilon)^{\frac{1}{2}}\,\frac{J_1(a\,r)}{r\,J_o(a\,r)}$$

$$n(r) = R\,\frac{i\phi}{riz} = R\left(\frac{n_o}{m_o}\right)^{\frac{1}{2}}\frac{J_1(a\,r)}{r\,J_o(a\,r)} = R\,(1+\varepsilon)^{-\frac{1}{2}}\,\frac{J_1(a\,r)}{r\,J_o(a\,r)}$$

The m- and n-functions have the same analytical form and differ only by the constant factor $1+\varepsilon$. This fact is in agreement with the "fluid" model.

The curves are given graphically in Fig. 3 for the case $\varepsilon = 0.33$ together with the line $n = \text{constant} = n_o$, which was the fundamental assumption for the "fluid" model.

As the two models are now seen to be very different (see Fig. 3) it should be possible to decide which is the better approximation.

It may perhaps be stated already here that the Bessel function model gives somewhat better agreement except in two cases: (a) a the lowest θ-values investigated where the models coincide, i.e. in the cases when n_o and hence also the parameter $\frac{n_o r}{R}$ are so small that the n-curves of the models differ very little (see Fig. 3); (b) just before and during the oscillating irreproducible stage of the discharge for which the fundamental assumption n = constant of the "fluid" model seems to be true.

The Bessel function model is incomplete in this respect that it has not been given a full physical explanation except in the force free case. However, the experiments will show that attempts directed towards a more general explanation are hardly worth while since the Bessel function model, like any other model, must be a rather rough approximation and further, that there are too many features which can be explained better and more simply than by a model.

2d. The axial flux conservation

It is known that very little axial magnetic flux penetrates the thick metal walls of the torus during the discharge. The total z-flux of the torus tube must therefore remain equal to the initial static flux $\pi a^2 B_i$. If the whole axial flux is captured by a known magnetic configuration with $B_z = f(I_z)$ and within a "cut off" radius b, i.e.

$$\int_0^b B_z \; 2\pi r \, dr = \pi a^2 B_i \qquad \ldots\ldots 5.$$

a relation between b, B_i and I_z can be obtained. However, such a relation is of limited value since it has been found that equation 5 is not a very good general approximation. There are two reasons for this : A well-defined "cut off" radius does not exist and, depending upon the discharge conditions, the plasma channel seems to be able to contain both more or less z-flux than the initial. When the plasma contains more flux, occurring at high θ-values, a reversed z-field appears outside the plasma channel. All model configurations have failed to explain this phenomena. It will be discussed later in connection with the experimental results.

However, Lees and Rusbridge have shown that a configuration model based upon the parameter θ = const. $\frac{I_z}{B_i}$ obtained from the equation 5 agrees well with the experiment in the case of low pinching, $\theta < 1.3$. The same equation together with the force free "fluid" model can be used to explain results concerning the oscillating "equilibrium" configuration, i.e. conditions at peak main current when the applied electric field is zero.

2e. The channel surface region

The experiments show that an axial flux is trapped in a concentrated magnetic configuration and surface currents may therefore be expected. The analysis giving the n(r)-curve provides a sensitive method to investigate the existence of more or less diffused skin currents on the surface of the plasma channel. If the B_z-field rapidly falls off outside a certain radius, a region of skin current in the ϕ-direction must also exist there. This fact is seen by applying the formula $\oint H.\underline{dl} = I$ along a contour going both outside and inside the fall off region. Such a border region implies a distinct change of the current direction and it can be seen as peaks at the ends of the n(r)-curve.

No definite indications of an initial skin current or separated magnetic fields have been found in the investigated cases, and this cannot be expected as earlier investigations have shown that the diffusion time of the magnetic fields is very short.

3. THE EXPERIMENTAL RESULTS AND THEIR INTERPRETATION

Before the detailed analysis of the discharge types, i.e. the m- and n- curves, is presented, it will prove advantageous to give results from simpler and more direct methods in order to explain the configuration just before the onset of large instabilities.

3a. The onset of large instabilities. Experimental facts

The discharge types studied are shown in figs. 4 - 6. These are followed by a number of figures (7 - 22) illustrating their magnetic field characteristics and analysis by the above means. In these figures the points for m(r) are shown by a dot, those for n(r) by crosses.

For discharges with B_i = 50 gauss (see discharges A and C) the onset of large instabilities has several characteristic features which are both evident and reproducible. The following observations have been made.

The unstable and irreproducible part of the discharge is always preceded by a change of the configuration rate of change. It is seen most conveniently on all oscillogram traces referring to B_z inside the plasma channel. A sudden decrease of the slope occurs ≈ 20 μs before the traces become clearly irreproducible. (See top trace in Fig. 4. This picture refers to discharge A, B_z at r =-3 cm.) The change of slope seems to occur slightly earlier for the outer part of the plasma than for the centre, but this difference is small, ≈ 5 μ s. The B_ρ - traces also show a change, but this is not fully as definite, neither in time nor in magnitude. No sudden variation is seen on the main traces (see bottom trace of Figs. 4 - 6) but as the Rogowski coil is separated from the plasma by the thick torus wall, a small sudden variation can hardly be expected to be recorded.

After the slope decrease has occurred the current helix system seems to become "rigid", i.e. $\bar{n}$ takes a constant value although the main current and the field components are still increasing. This fact is clearly seen from Fig. 11. It should be remembered that ΔB_z is the maximum field strength minus the average of the two minimum strengths B_{-12} and B_{15} and that ΔB_z is therefore directly proportional to the total channel ϕ -current I_ϕ. Experimental curves to be discussed later will prove that the z-current existing outside the plasma channel is small for discharges A and C and thus that the straight portion $\bar{n}$ = 7.7 really represents a "rigid" configuration i.e. a constant ratio I_ϕ/I_z for

the plasma channel.

It should also be noticed that a negative, reversed z-field appears just when the current configuration becomes "rigid".

The curves corresponding to Figs. 11 and 12 are not shown for discharge C because they are quite similar apart from giving another value for $\bar{n}$, which in case C is 8.8.

The $\bar{n}$-curve of Fig. 12 is deduced from ΔB_z of Fig. 11 and compared with the centre magnetic turn number m(o). The "rigid" time period of $\bar{n}$ between 90 and 110 μs does not seem to have a counterpart in the magnetic helix system.

The "rigid" configuration is unstable or rather, it seems to accept only a limited increase of the main current I_z before it becomes irreproducible. At this stage the regular oscillations, extensively described in an earlier paper[3], often begin to occur, especially for fast current rise discharges, i.e. high θ_p-values. As the analysing methods used here are then no longer valid, the curve parts which refer to distinctly oscillating or irreproducible conditions have been drawn in hatched regions. (Figs. 11 and 12).

The observations given here have no direct correspondance in case of the low pinched discharge B. By comparing the top traces of the oscillograms, Fig. 4 - 6, it is seen that the instabilities in case B have neither the definite onset nor are they as violent. The n- and m- curves will show that a considerable part of the main current I_z goes outside the plasma channel and also that the definitely "rigid" current configuration does not seem to exist in this case. This can be seen by comparing Figs. 11 and 17.

3b. The onset of large instabilities. Explanation

The earlier investigation, "Regular Oscillations in Toroidal Discharges", reference 3, provides a framework for discussion of the above - mentioned observations. There it is proved that the regular oscillations are connected with an inhomogeneous current density distribution, causing a large part of the main current to be excluded from a helical notch of the plasma channel.

The most likely explanation of the "rigid" current configuration is as follows. The increase of the main current I_z during the "rigid" period is restricted only to a certain helical path which closes upon itself, i.e. the n- number of the path is integral. The measured average turn number $\bar{n}$ must

then remain constant although other quantities as magnetic field strength, trapped flux etc. increase.

The helical current notch is wound so as to increase the trapped magnetic flux and the outer ε-field must accordingly decrease and even become negative because of the axial flux conservation. The notch current thus provides the necessary asymmetry since no cylindrically symmetric configuration model has been found able to cause a reversed B_z-field.

It is easily understood that an exact experimental determination of the notch turn number is not possible with the use of magnetic probes only. For three discharges with respectively θp = 2.07, 2.50 and 3.05 the "rigid" $\bar{n}$-numbers have been found to be 6.5, 7.7 and 8.8, and these figures, which may indicate the actual turn numbers 7, 8 and 9, are in good agreement with results from the earlier investigation[3].

3c. Discharge A

The discharge A (see Fig. 4, Figs. 7 - 12 and Table I) clearly depicts many characteristics of a medium discharge but also the difficulties and imperfections of the measuring and analysing methods. For the n- points near the centre (Figs. 8 -10, the lower curves), it has to be considered that the probe dimension is almost of the same order of magnitude as the investigated region. Unfortunately the B -configuration point differences $\delta(B_z)$ are very small here and the errors of the n- curve points are accordingly large.

It is very difficult to analyse and correct the configuration perturbations which are caused by the probe. No attempt has been made to correct the results presented here as future experiments with different probe sizes can give the only simple and reliable answer about the probe influence.

No theoretical model can be applied very successfully to the A-configurations as the basic condition of symmetry is poorly fulfilled and the deviations do not seem to be caused by the toroidal geometry only. The technique of comparison with model configurations here shows its limitations but if an attempt to use it were made, the Bessel function model would probably be the best approximation in the cases AI and AII (cf. Figs. 2 and 3). However, only the central part of the region where $J_o(\alpha\, r) > 0$ can be used.

The degree of pinching, i.e. the difference between the m- and n- curves is fairly constant in time and also in space apart from a deviation seen on the configuration A II which illustrates the conditions just at the beginning of the "rigid" period. The small force free region (m = n) may be due to the notch current.

A III is obtained just before the onset of large instabilities. At this stage a "fluid" model, i.e. n is constant, is the best approximation. A III is too unsymmetrical to show this fact very clearly, but a somewhat slower discharge type D, not very different from A, gives a better picture of the conditions just before the oscillation period. The discharge D (see Fig. 22) is not fully presented here as it gives practically the same information as A. For D the peak current θ-value is 2.07 and for A it is 2.50. The initial fields are the same, 50 gauss.

3d. Discharge B

The $\bar{n}$ lines here are always lower than an average of the n-points (see Figs. 14 - 16) which shows that a z-current is going outside the plasma channel. This fact can also be seen from the $B\phi$ -curves (Fig. 13) which, at least for the cases BI and BII, do not look like those of a vacuum field near the wall.

Both n and $\bar{n}$ seem to increase continuously with time.

In the case BI the n-curve has a strong deviation. Although n-curve "jumps" of this kind have been found for other similar discharges, the deviation is probably due to a very small variation in the discharge conditions, affecting, but hardly seen on, the z-component curve and then causing the large "jump".

For BII the experimental point differences are larger and accordingly the n-curve is more reliable. The gas pressure variation is not symmetrical as seen from the distance between the n- and m- curves.

The earlier investigation about regular oscillations showed that the helical current notch seems to rotate around the magnetic centre line. The analysing methods used here are not very suitable to prove similar facts, but it has been found that a force free region of the plasma, like that of BII, to the right of the centre, does not remain in the same position. The force free region of B III, left hand side, is the development of the corresponding BII region.

At the stage B III, the discharge has just begun to be irreproducible. The configuration is rather unsymmetrical and to a large extent force free.

3e. Discharge C

Discharge C is the case with the fastest investigated current rise. The configurations CI and CII exhibit about the same features as those of discharge A but at earlier times after the start. The "rigid" configuration time is between 60 and 70 μs and the instabilities then occurring are extremely sudden and violent as seen from Fig. 6.

The configuration C III refers to a time a few μs before the onset of those large instabilities. There is a region where the pressure gradient seems to be directed outwards. This is probably a notch current region but magnetic probe measurements on such features must necessarily be rather uncertain.

Skin current regions discussed above are seen both in case A III and D III.

Within experimental error, the straight $\bar{n}$-line always seems to be a good average of the n-points, indicating that the z-current outside the channel is small.

4. SUMMARY AND CONCLUSIONS

Magnetic search coil measurements have been made on diffuse pinch discharges in the MK IV torus, which external and amplify previous observations[1]. The observed configurations have been compared with semi-empirical theoretical models and the Bessel function model, somewhat modified, has been found to be a fairly good approximation for that condition range where it was found valid in the previous investigation. For the later stage of the discharge the deduced "fluid" model is shown to be a better approximation, but as this report only concerns the reproducible part of the discharge, very little more can be said about that model.

However, the most important parts of this investigation are more indications than definite results. It is shown that the irreproducible and oscillating part of the discharge is always preceded by a very reproducible time period when the current configuration is "rigid". The "rigid" configuration is here simply explained by a narrow helical current notch closing upon itself. This view is supported by the appearance of the reversed z-field near the tube wall and by the $\bar{n}$-values reported. A definite proof could easily be obtained by measuring a large number of such $\bar{n}$-values in order to prove a tendency of "clustering" around integral values.

Due to the probe technique used only macroscopic electrical and magnetic properties of the plasma have been investigated and reported. Clearly other diagnostic methods are necessary in order to fully explain the problem of the onset of instabilities, e.g. how a runaway current channel is formed. This seems important since such a closed channel makes a continuous pinching process impossible.

ACKNOWLEDGEMENTS

I wish to thank the members of the probes section, i.e. D.J. Lees, H.W. Jones, M.G. Rusbridge and P.A.H. Saunders for advice and helpful discussions.

My year in England was made possible by a grant from the Swedish Natural Science Council.

REFERENCES

1. D.J. Lees, M.G. Rusbridge, Proc. Fourth Int. Conf. on Ioniz. Phenomena, Uppsala, p.954, (1959).
2. G.N. Harding et al. Geneva Conf. Paper P/1520 (1958).
3. M.G. Rusbridge et al. "Regular Oscillations in Toroidal Discharges", In press, to be published in J. Nucl. Energy, Part C.
4. S. Lundquist, Ark. Fys. 2 p.361, (1950).

Scales for the oscillograms

Figs. 4 and 6: 94.0 gauss/div.; 4.72 kA/div. ; 100 μs/div.

Fig. 5: 37.6 gauss/div.; 4.72 kA/div. ; 100 μs/div.

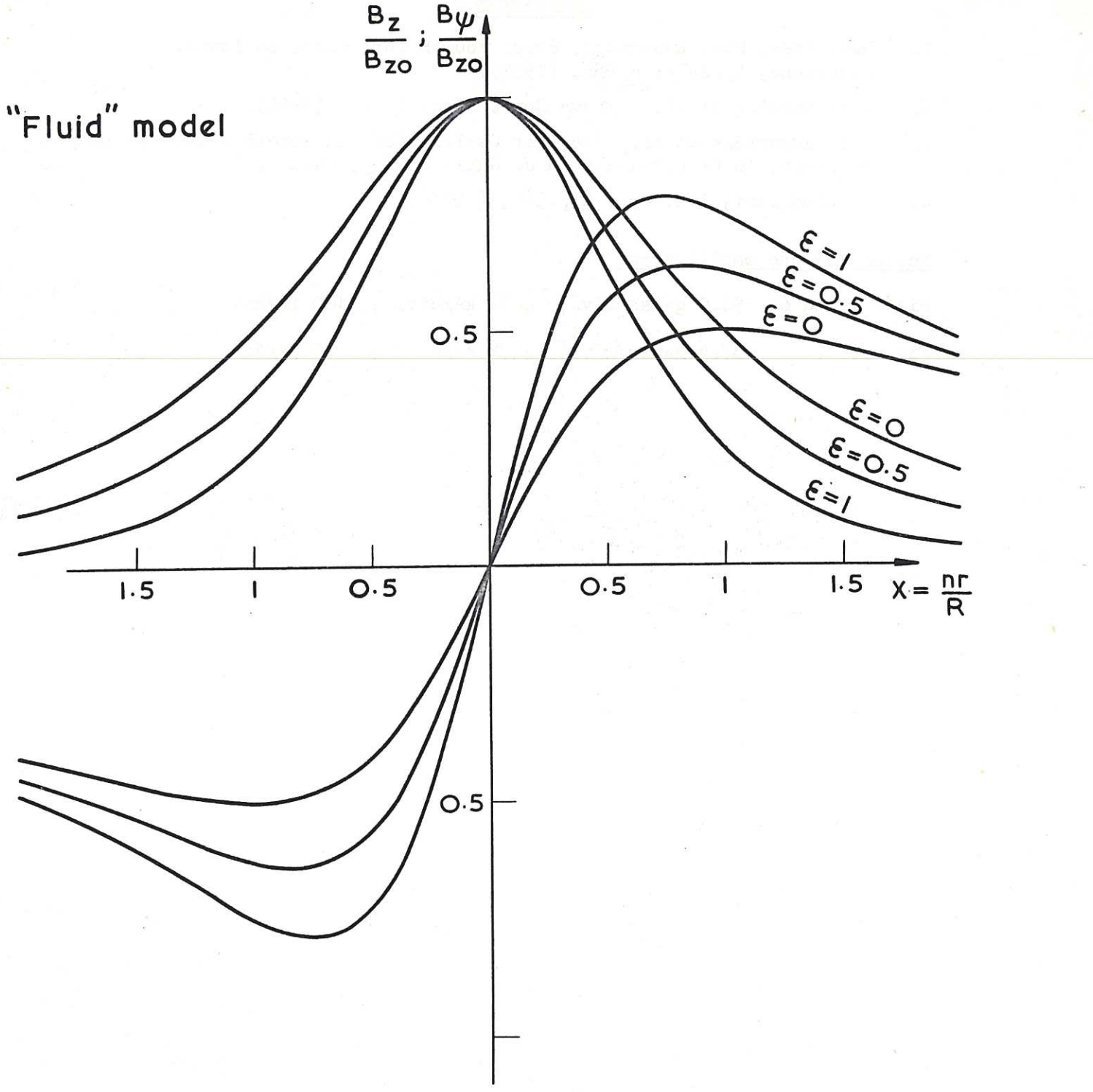

CLM - R7 Fig. 1
The "fluid" model for ε = 0, 0.5 and 1

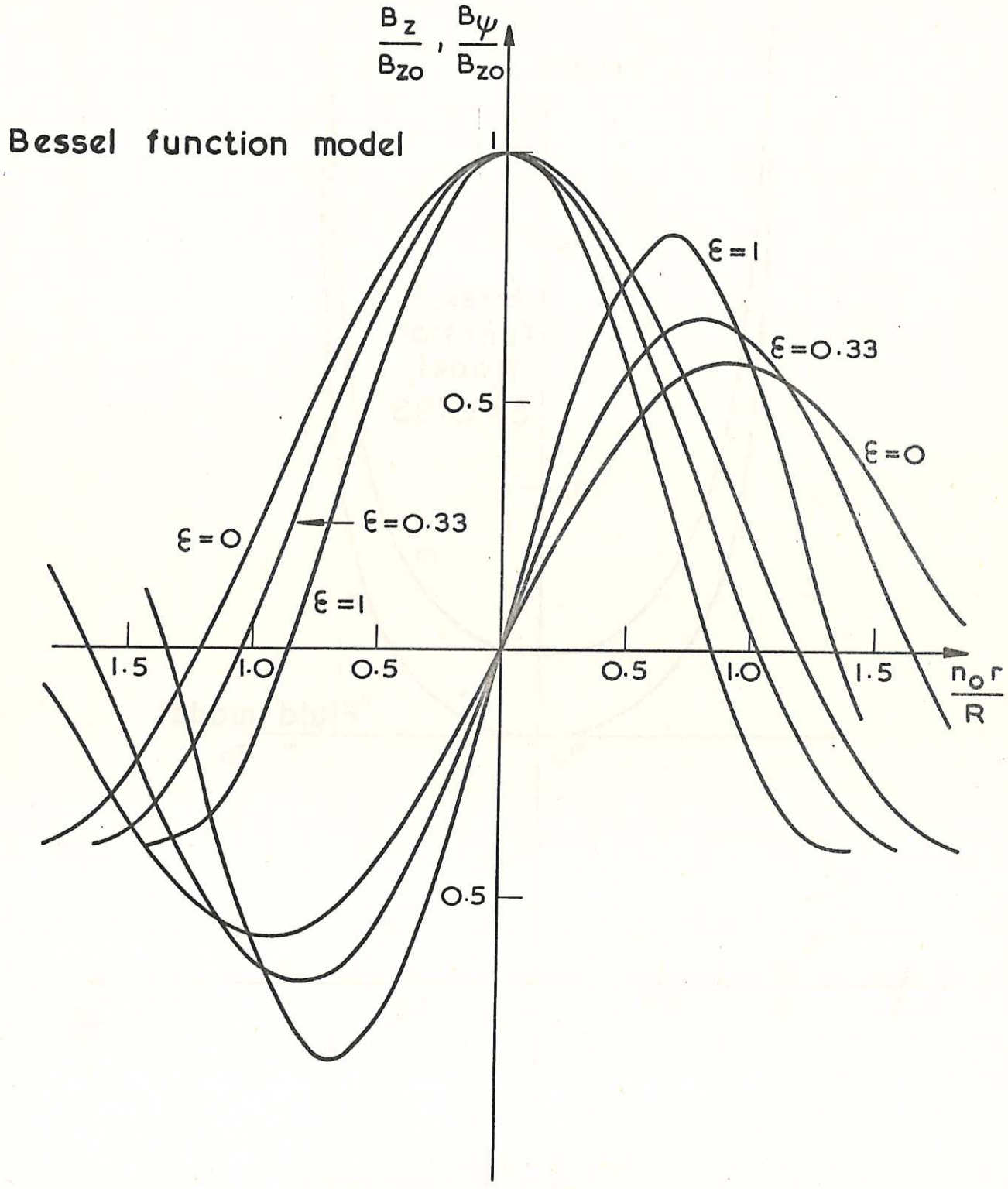

CLM - R7 Fig. 2
The Bessel function model for $\varepsilon = 0,\ 0.33$ and 1

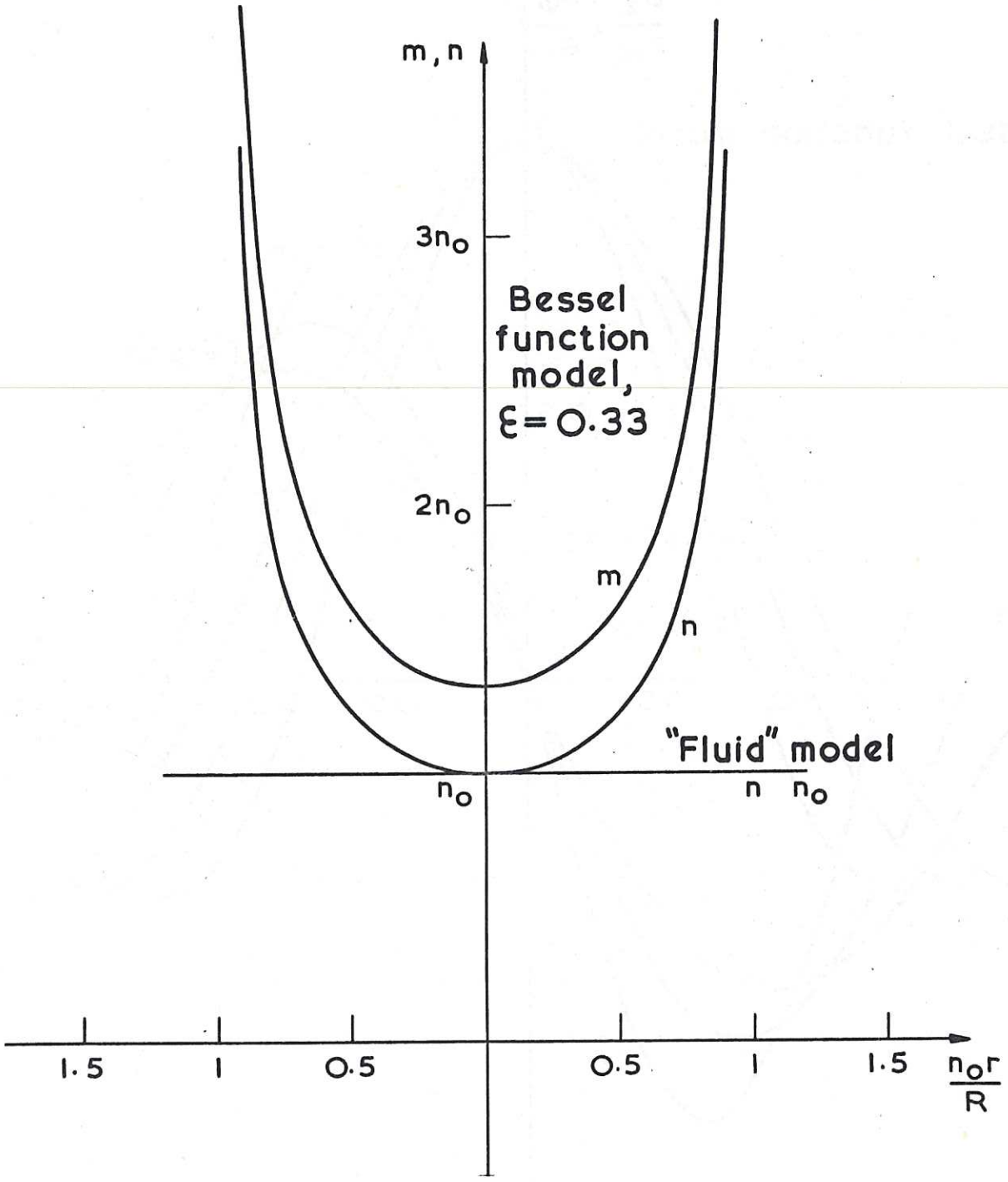

CLM - R7 Fig. 3
m- and n- curves from the theoretical models

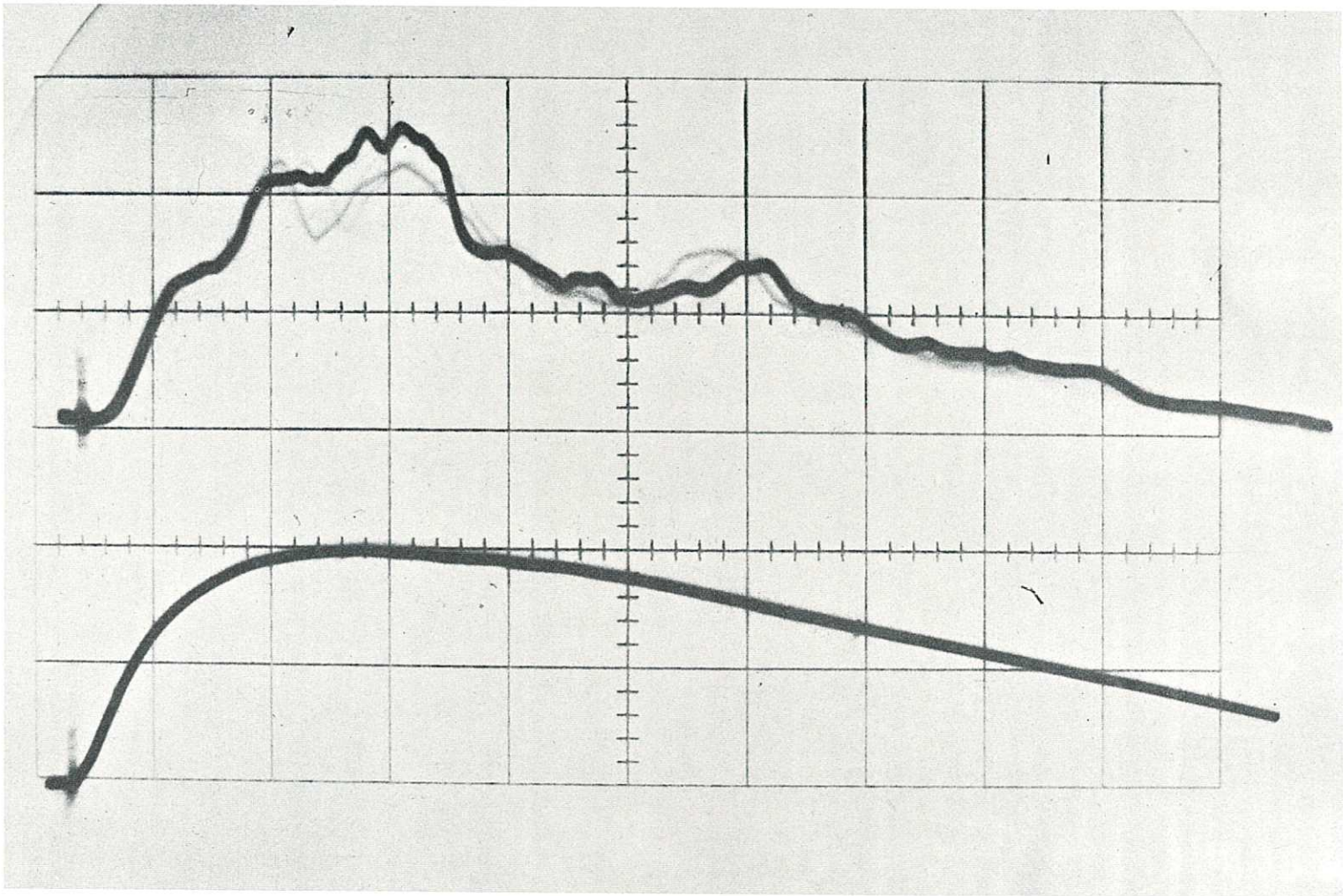

CLM - R7 Fig. 4
Oscillogram. Discharge A. B_z and I_z, r = -3 cm.

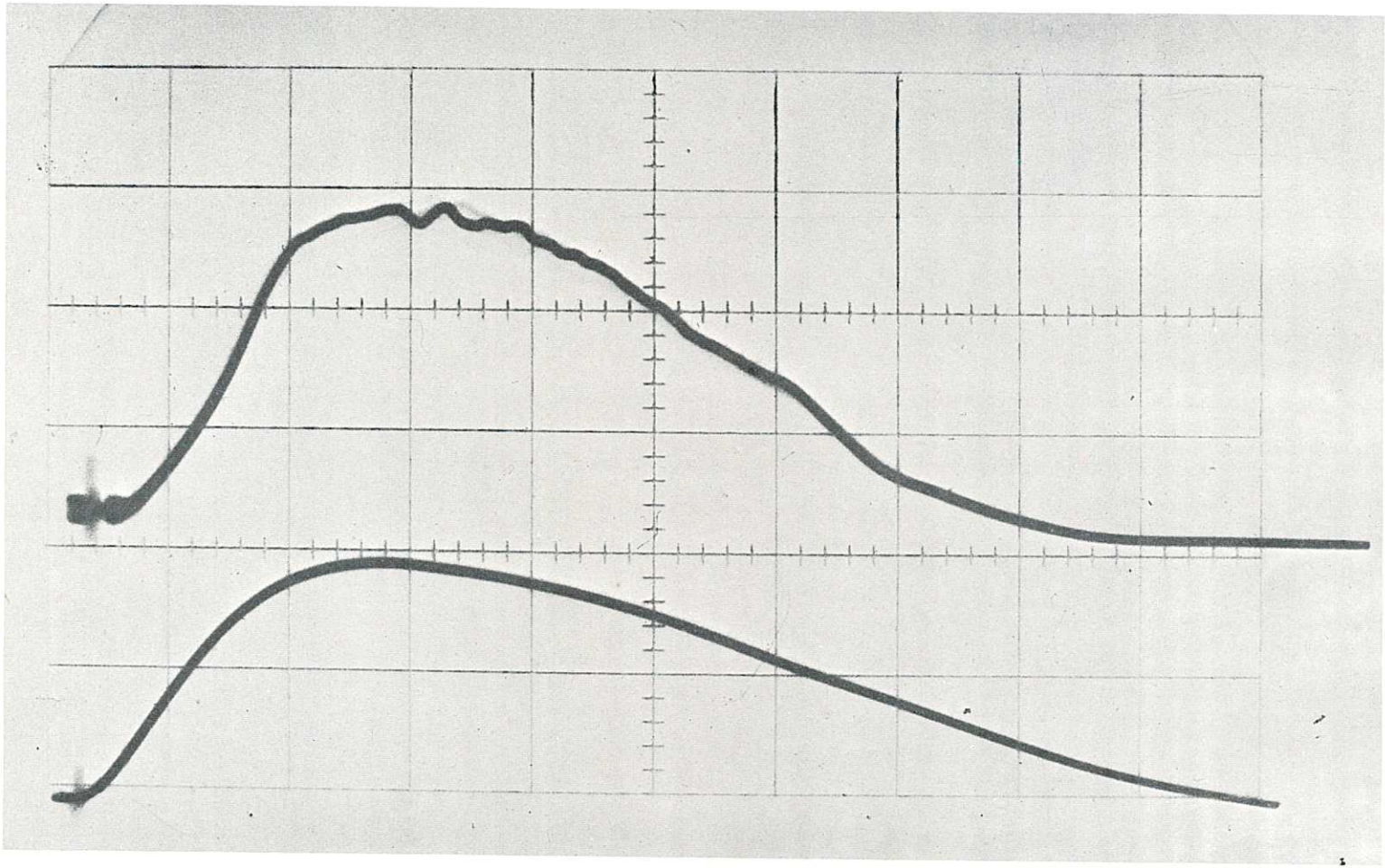

CLM - R7 Fig. 5
Oscillogram. Discharge B. B_z and I_z, r = 0

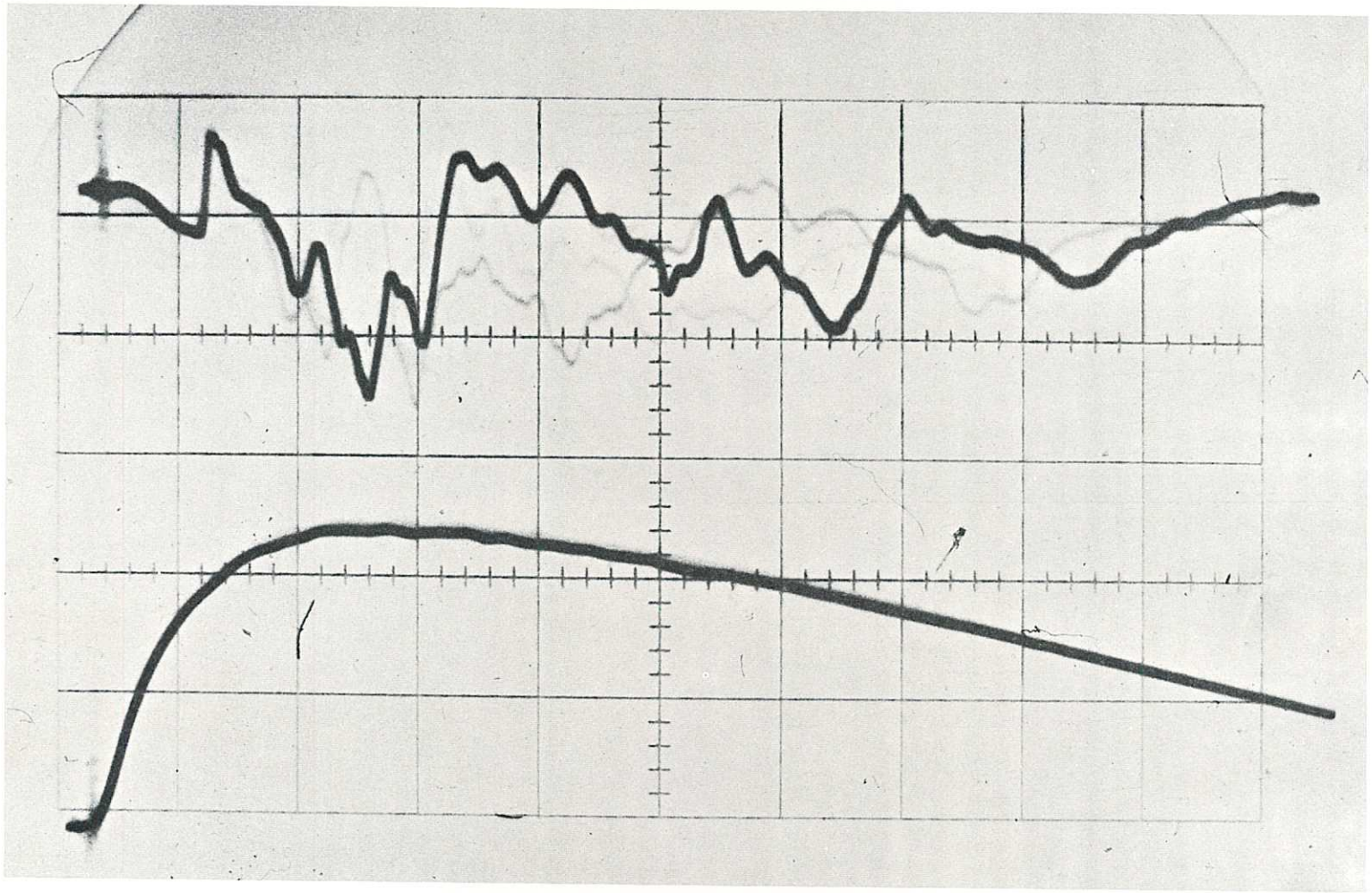

CLM - R7 Fig. 6
Oscillogram. Discharge C. B_ϕ and I_z, r = 2 cm.

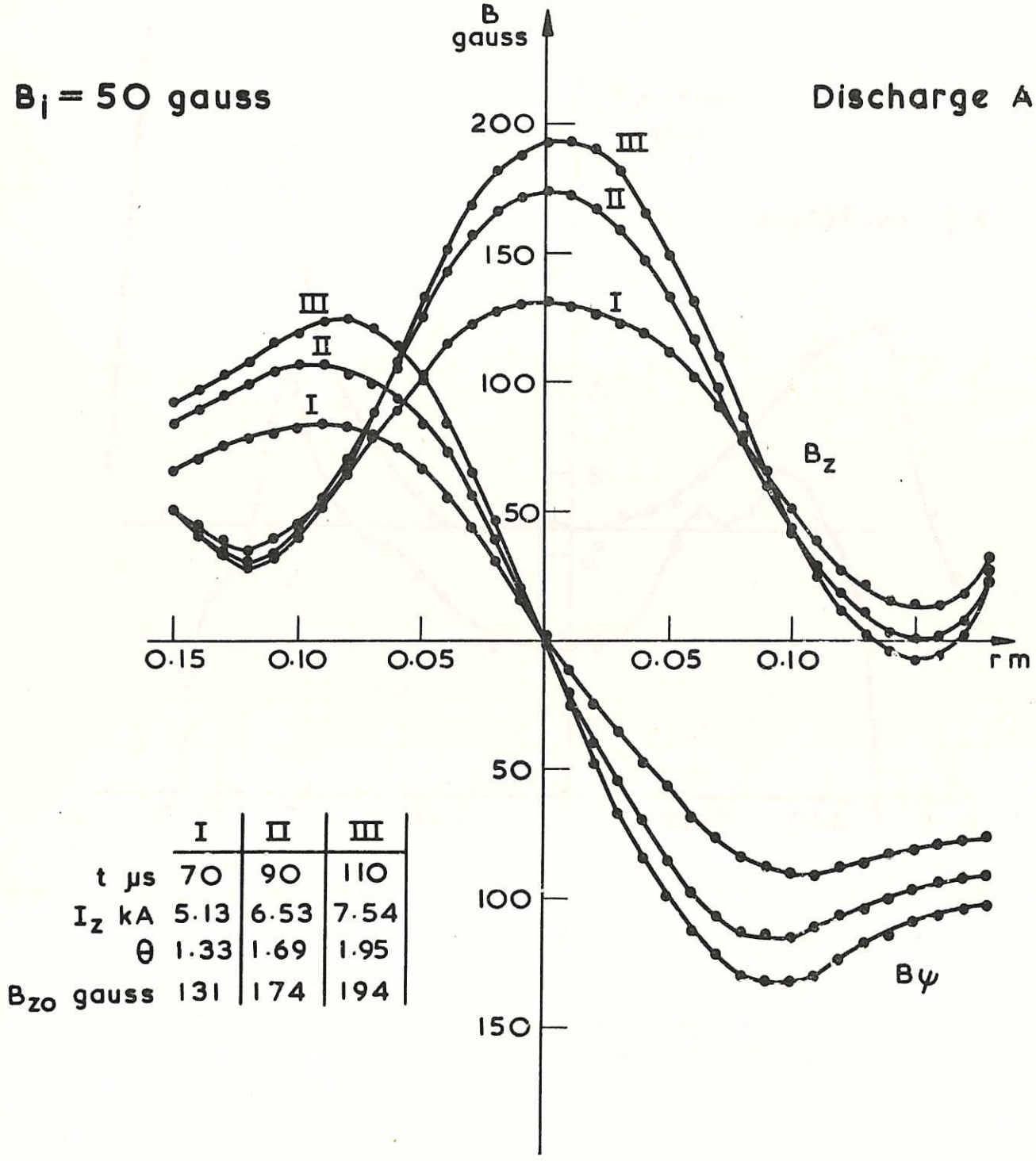

	I	II	III
t μs	70	90	110
I_z kA	5·13	6·53	7·54
θ	1·33	1·69	1·95
B_{zo} gauss	131	174	194

CLM - R7 Fig. 7
Field components for discharge A

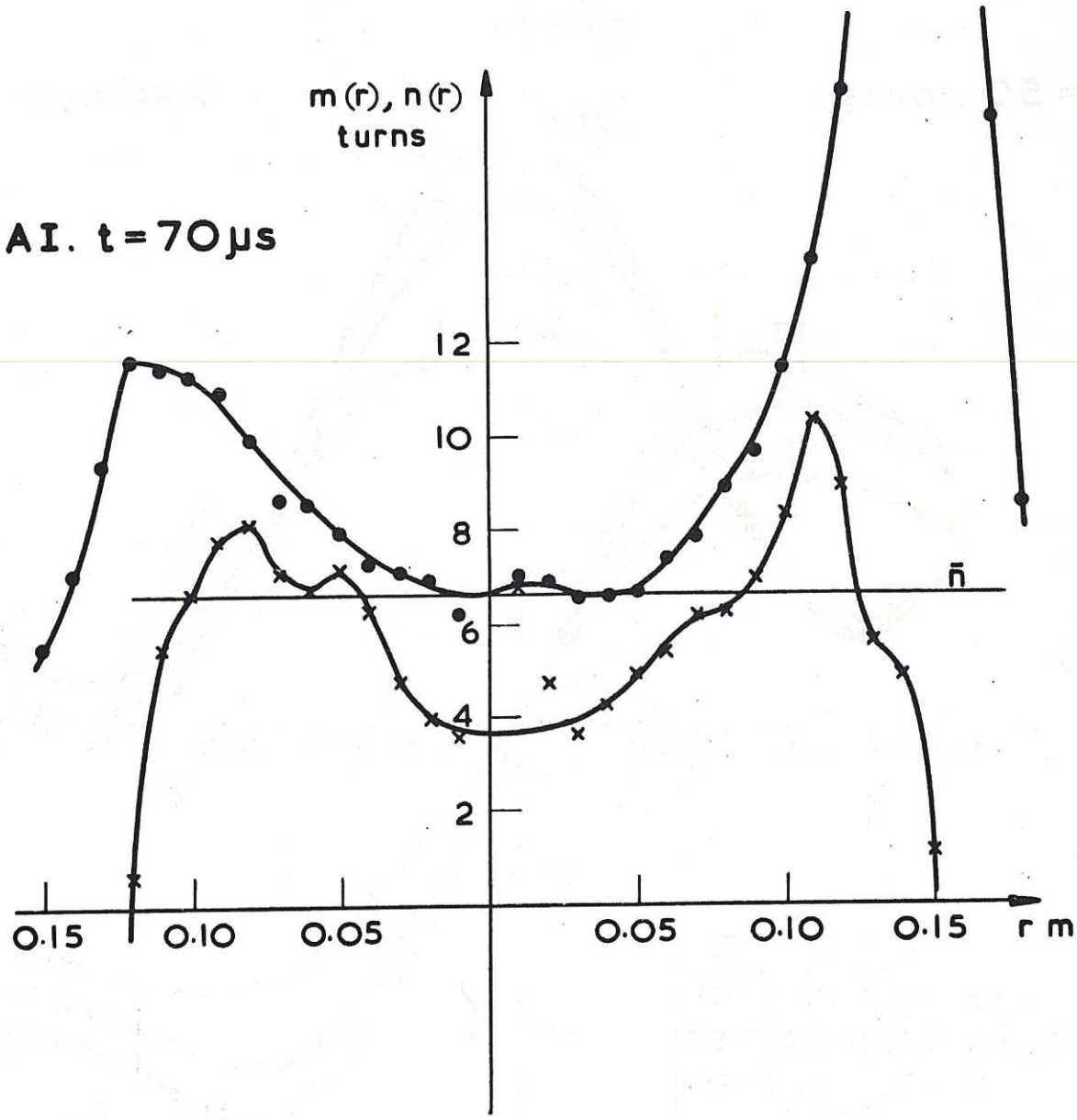

CLM - R7 Fig. 8
m- and n- curves for configuration AI

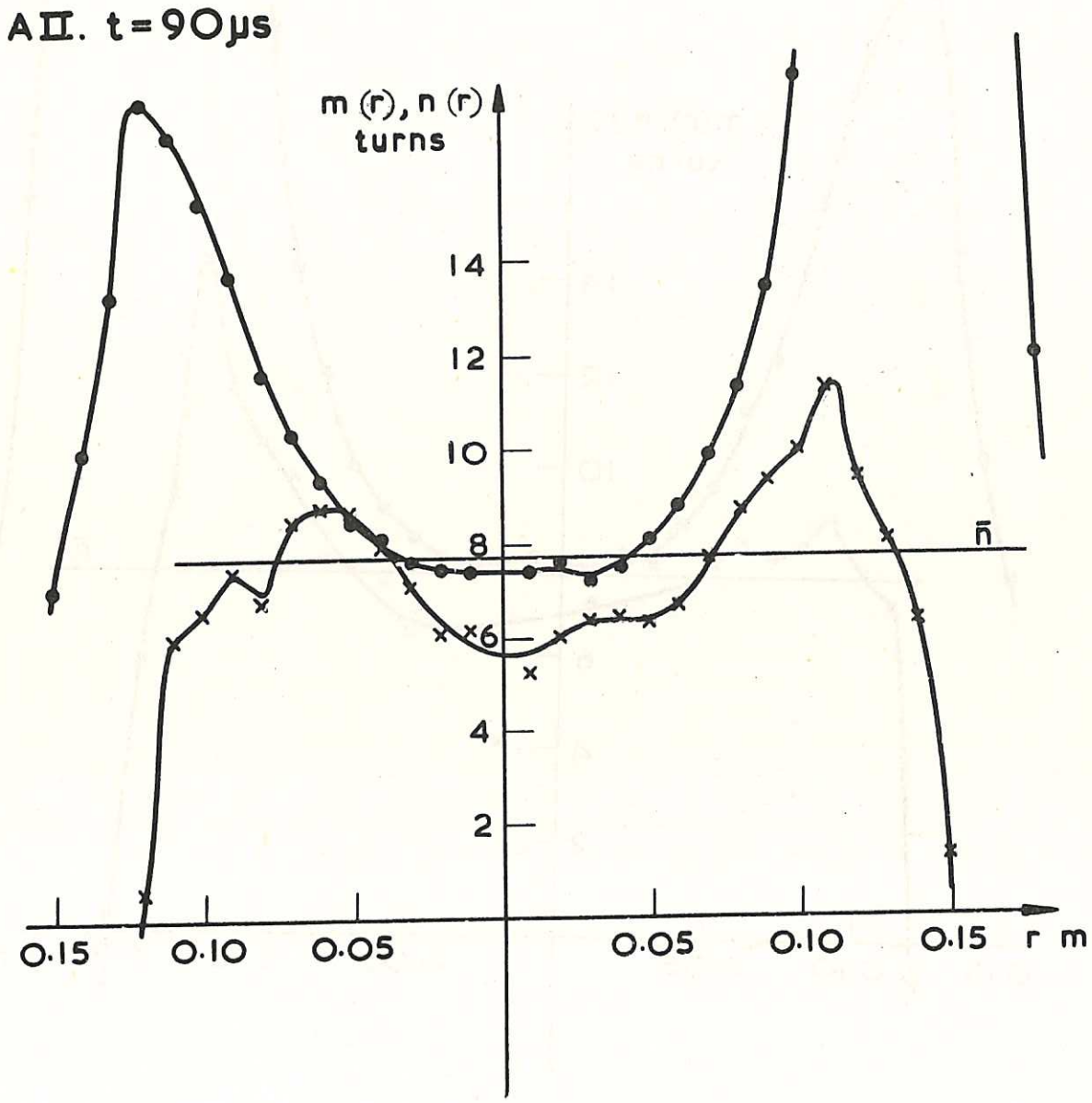

CLM - R7 Fig. 9
m- and n- curves for configuration AII

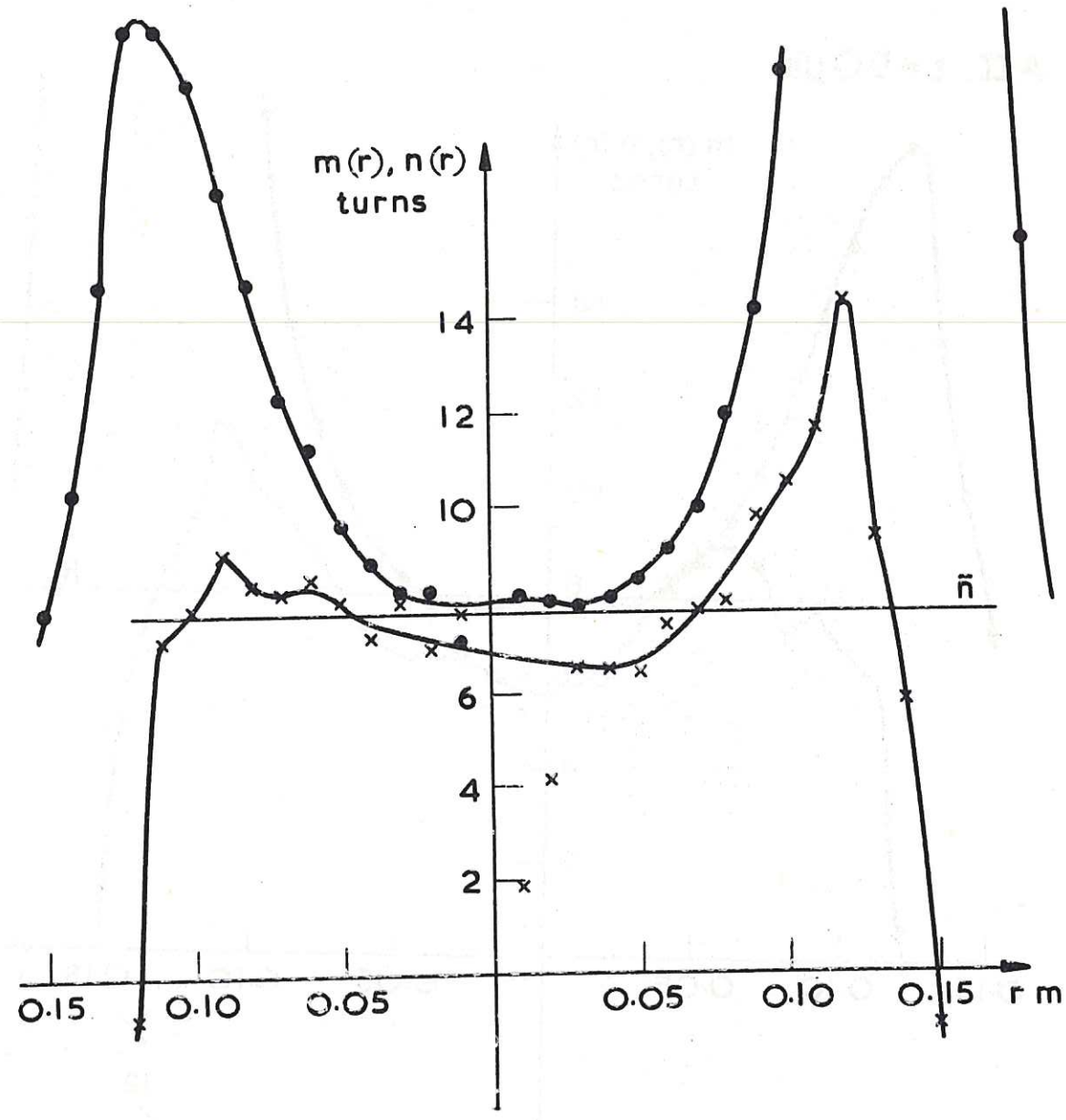

CLM - R7 Fig. 10
m- and n- curves for configuration AIII

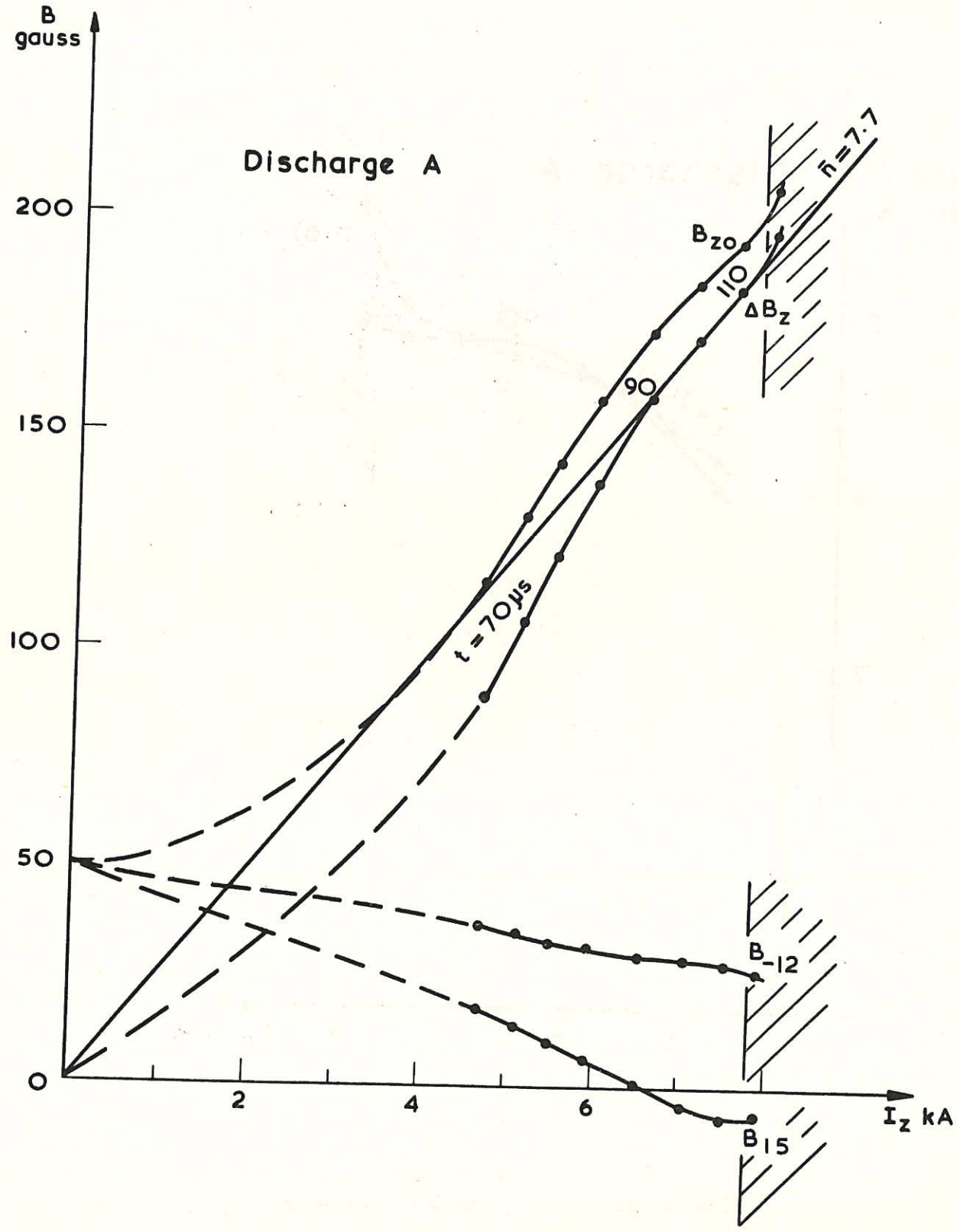

CLM - R7 Fig. 11

Discharge A. B_{zo}, ΔB_z and B_{min} as functions of I_z

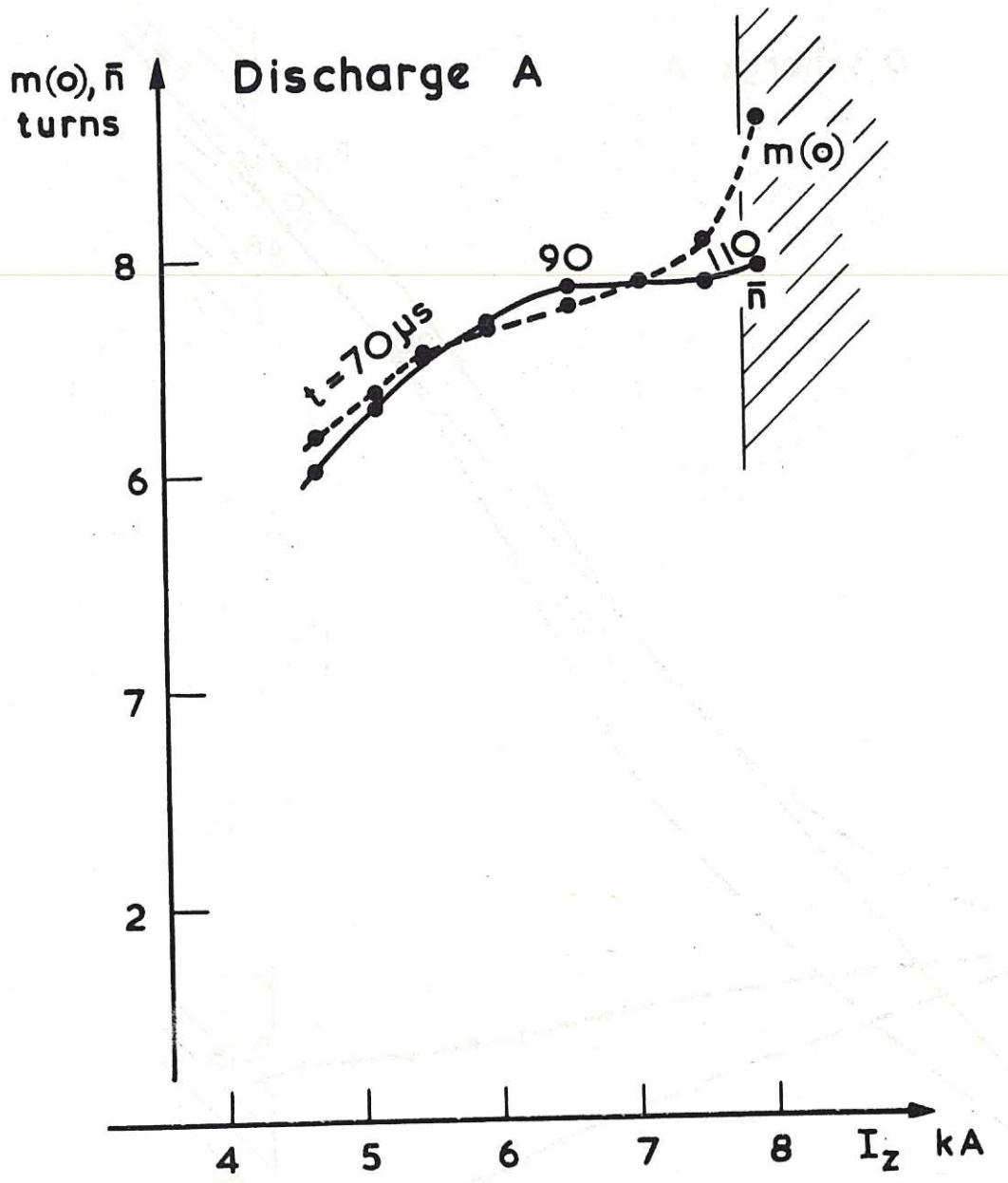

CLM - R7 Fig. 12
Discharge A. m(O) and $\bar{n}$ as functions of I_z

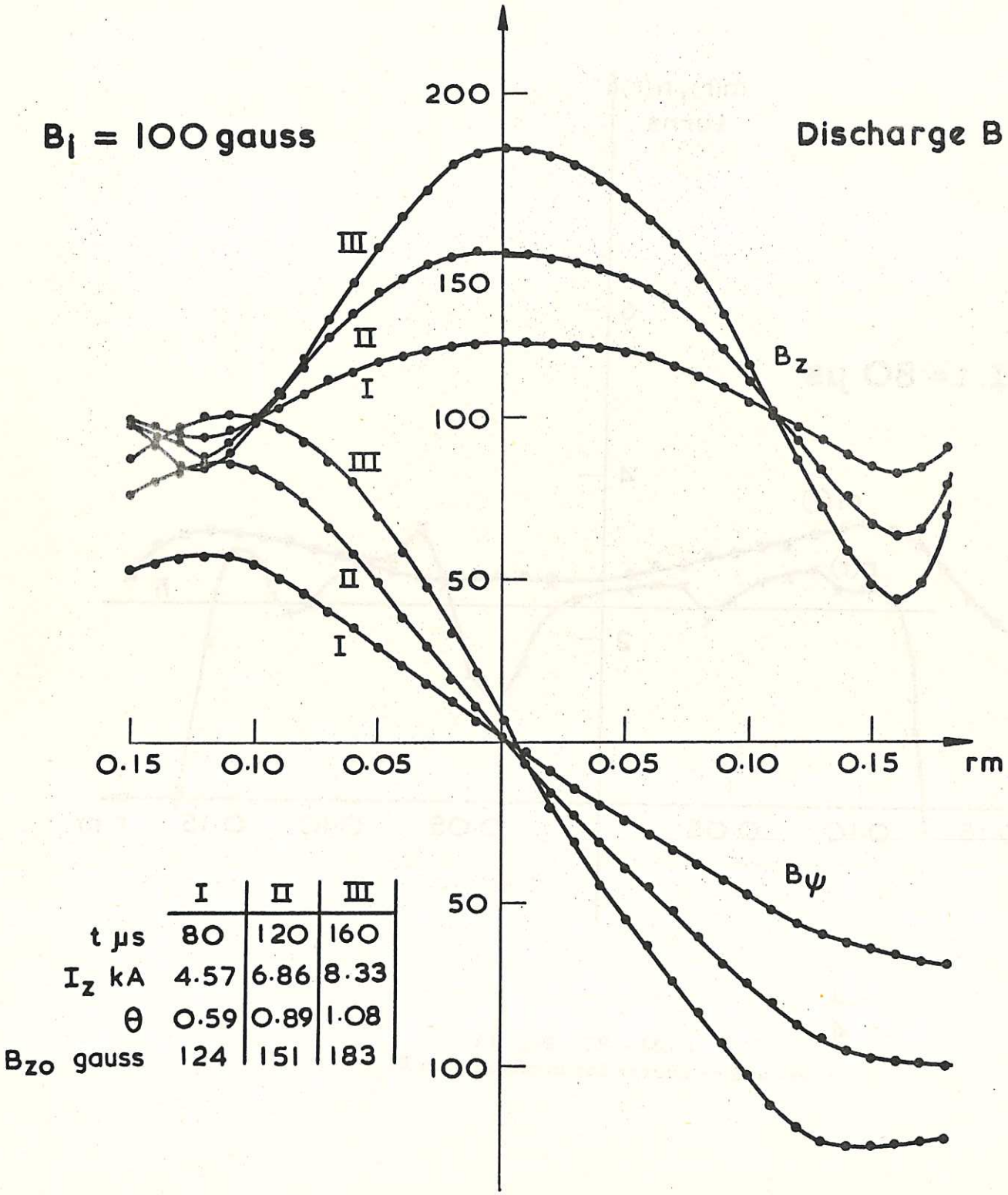

	I	II	III
t μs	80	120	160
I_z kA	4.57	6.86	8.33
θ	0.59	0.89	1.08
B_{zo} gauss	124	151	183

CLM - R7 Fig. 13
Field components for discharge B

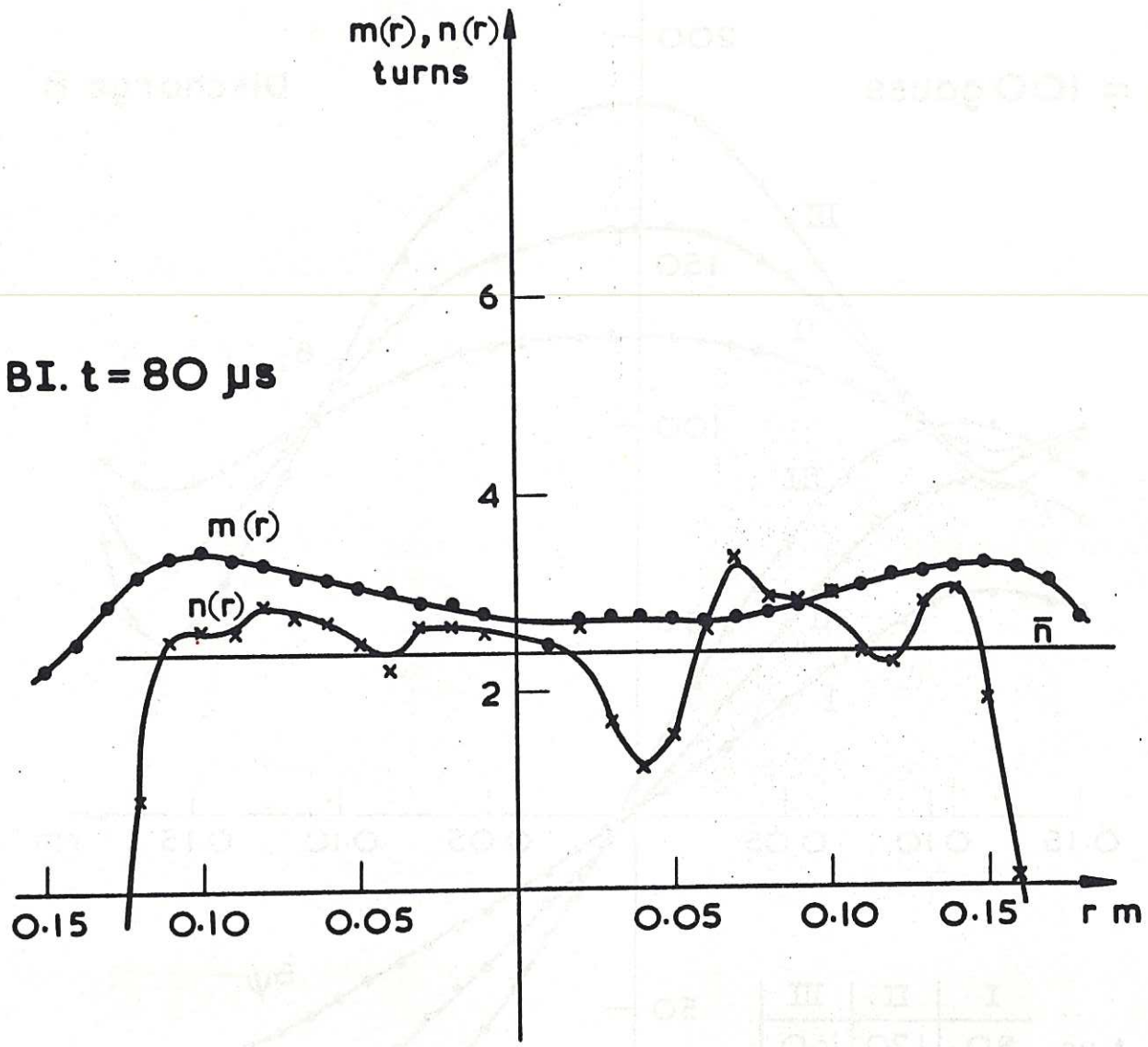

CLM - R7 Fig. 14
m- and n- curves for configuration BI

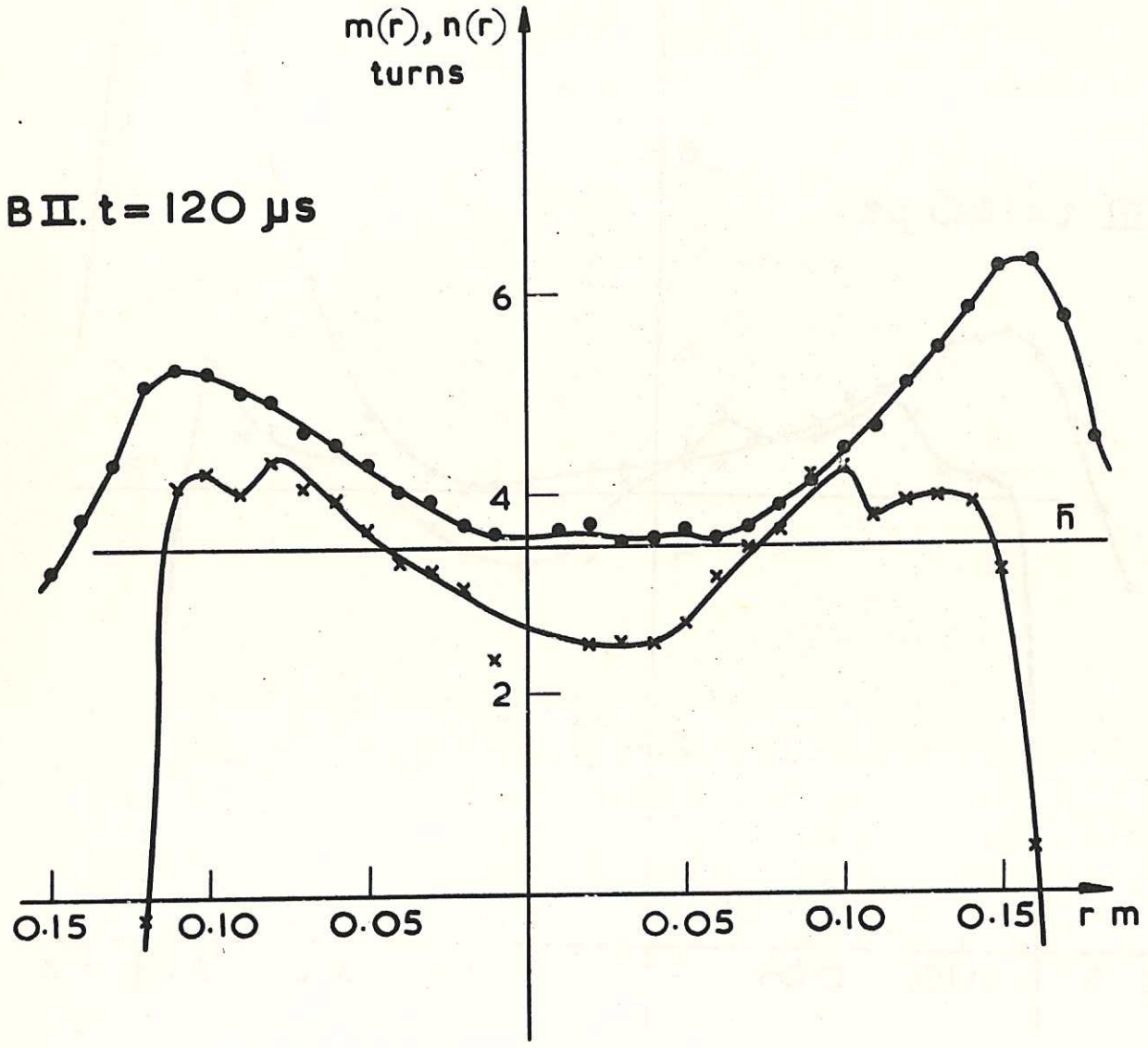

CLM - R7 Fig. 15
m- and n- curves for configuration BII

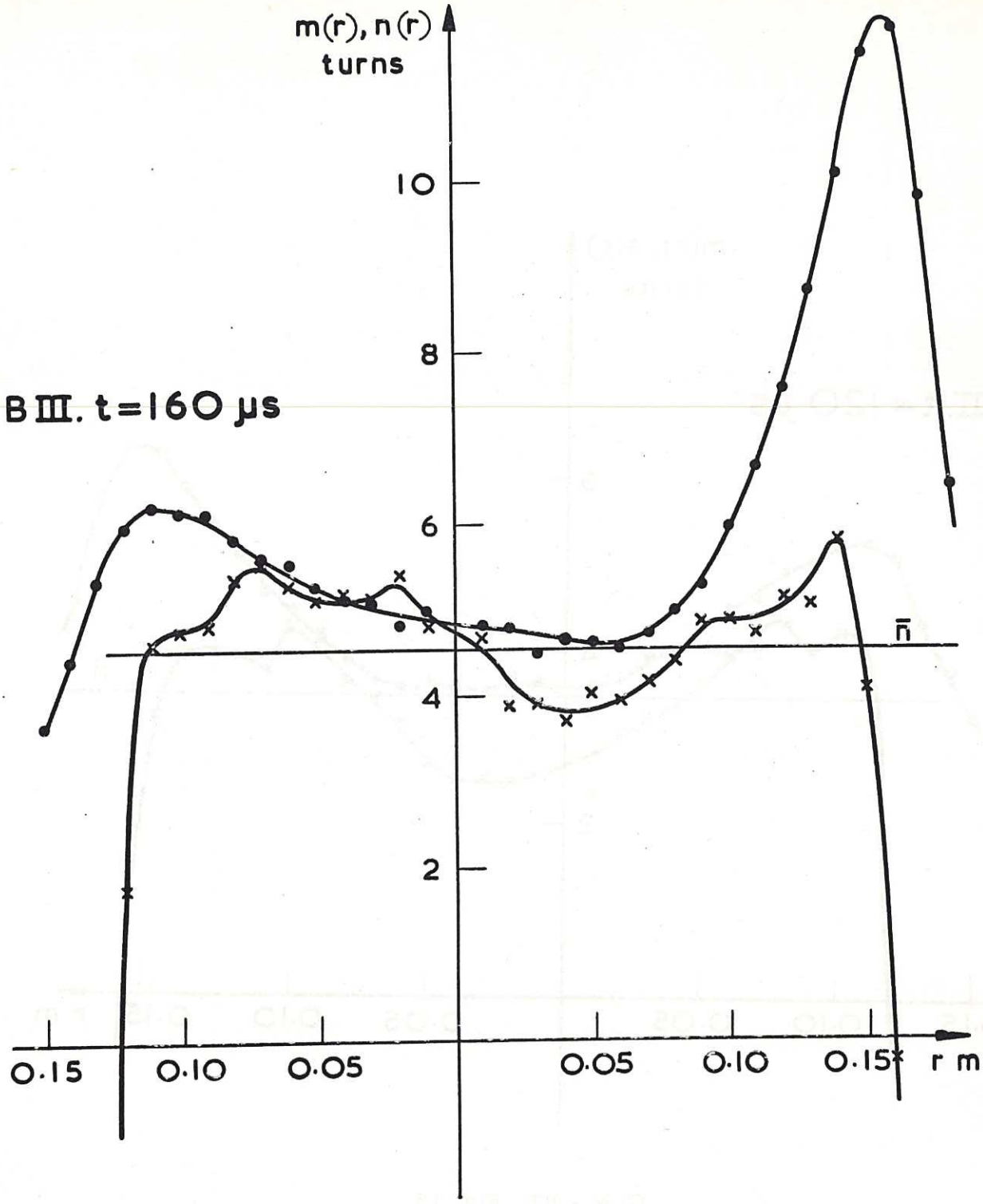

CLM - R7 Fig. 16
m- and n- curves for configuration BIII

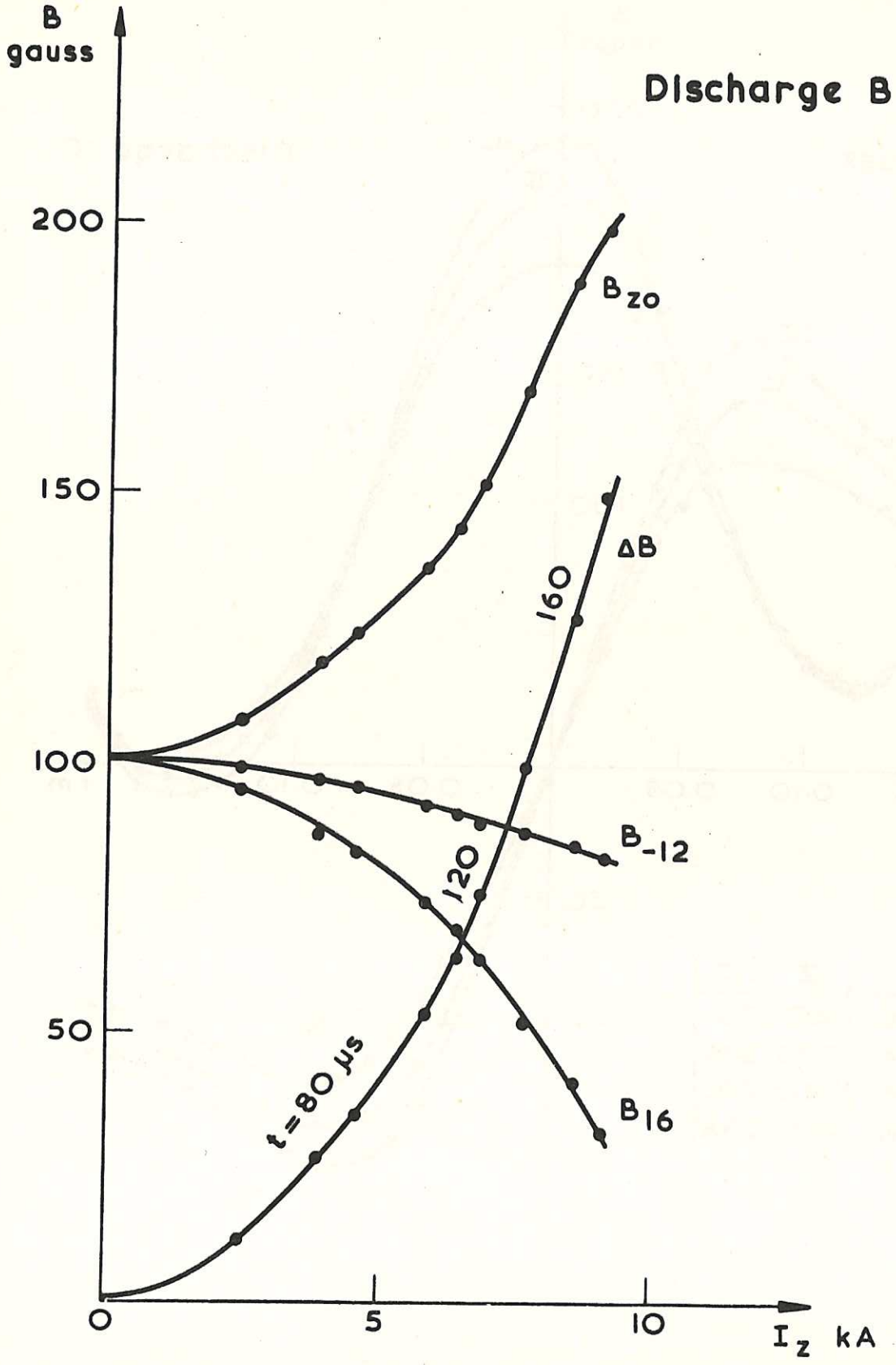

CLM - R7 Fig. 17

Discharge B. B_{zo}, ΔB_z and B_{min} as functions of I_z

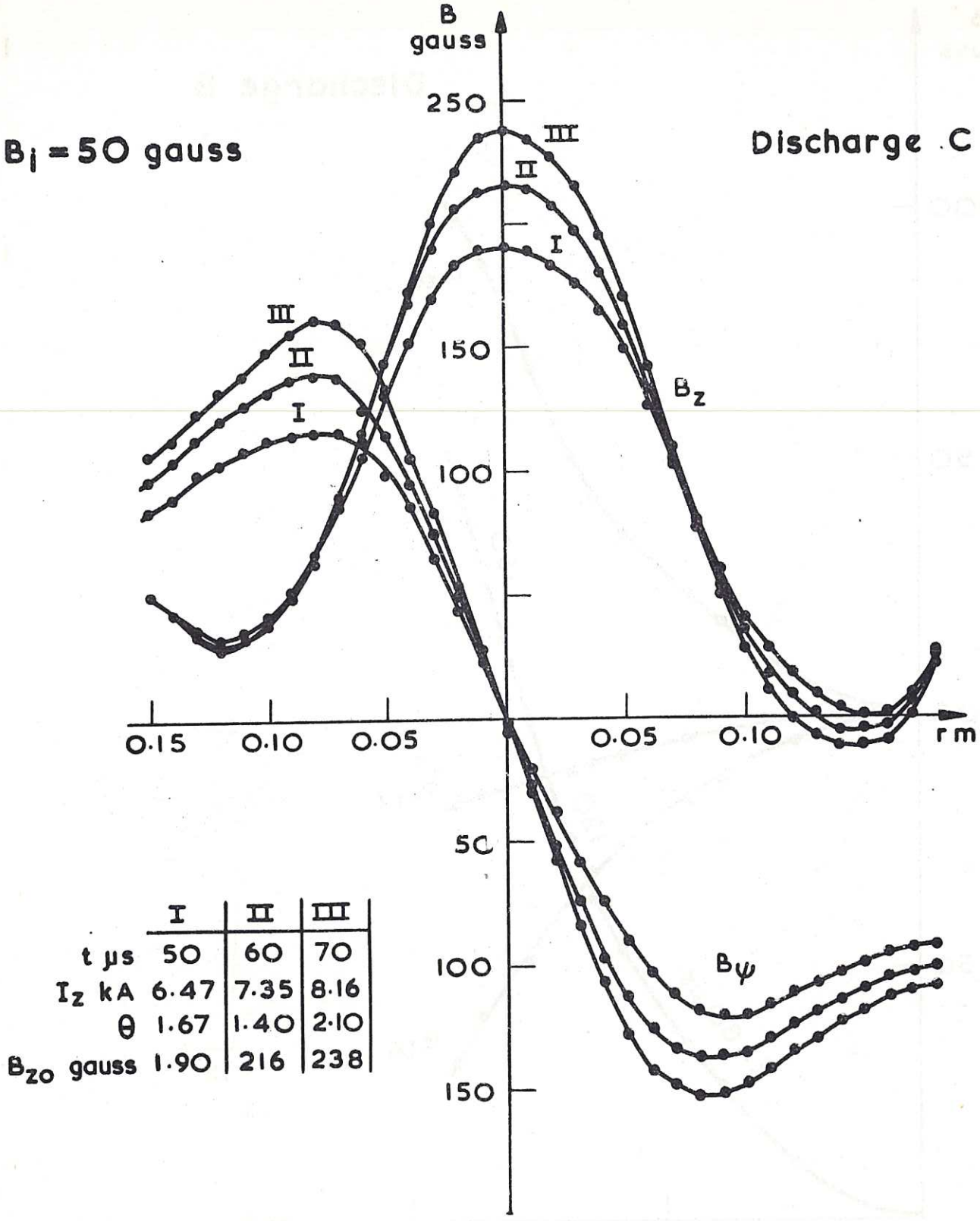

	I	II	III
t μs	50	60	70
I_z kA	6.47	7.35	8.16
θ	1.67	1.40	2.10
B_{zo} gauss	1.90	216	238

CLM - R7 Fig. 18
Field components for discharge C

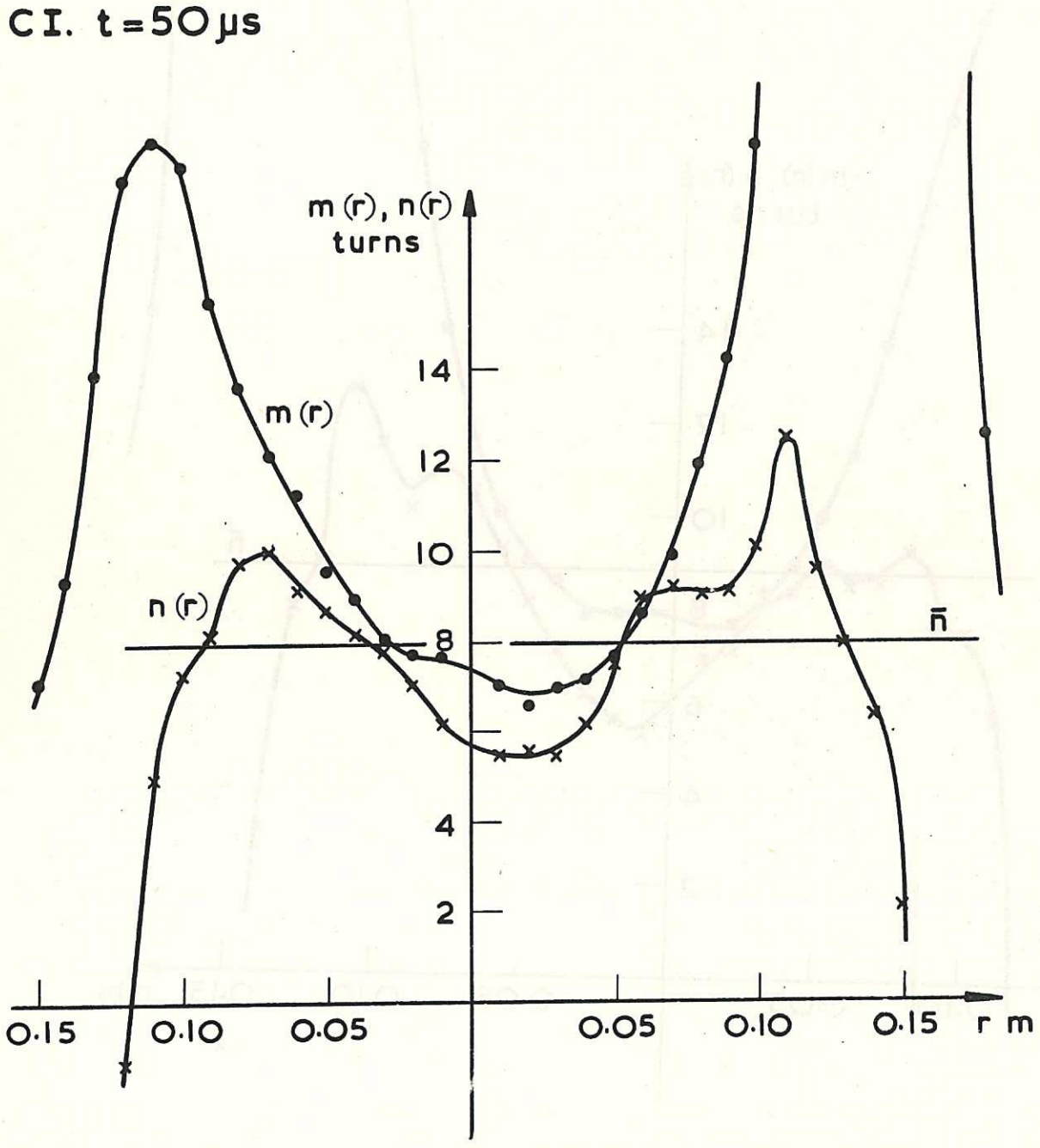

CLM - R7 Fig. 19
m- and n- curves for configuration CI

CII. t = 60 μs

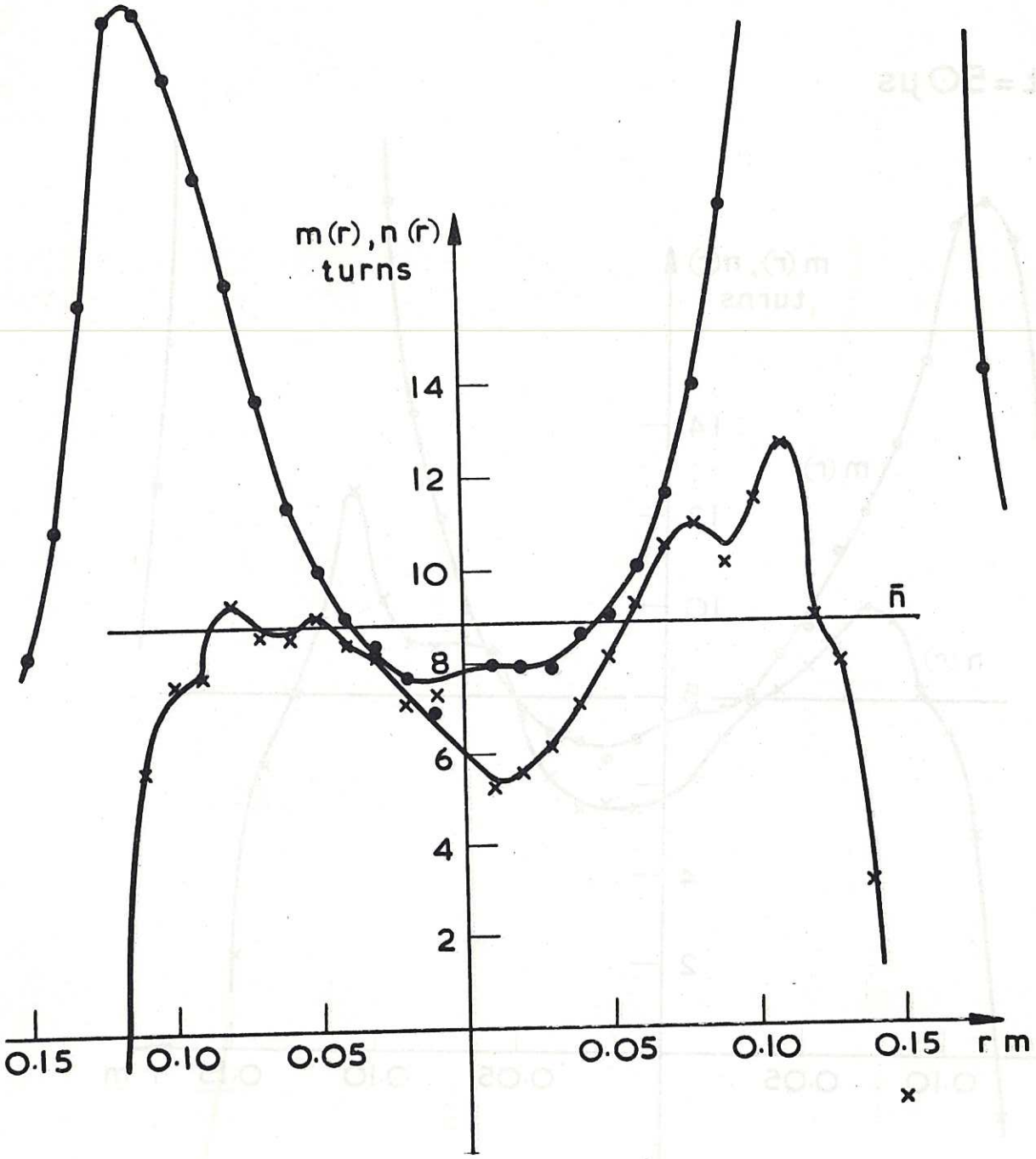

CLM - R7 Fig. 20
m- and n- curves for configuration CII

C III. t = 70 μs.

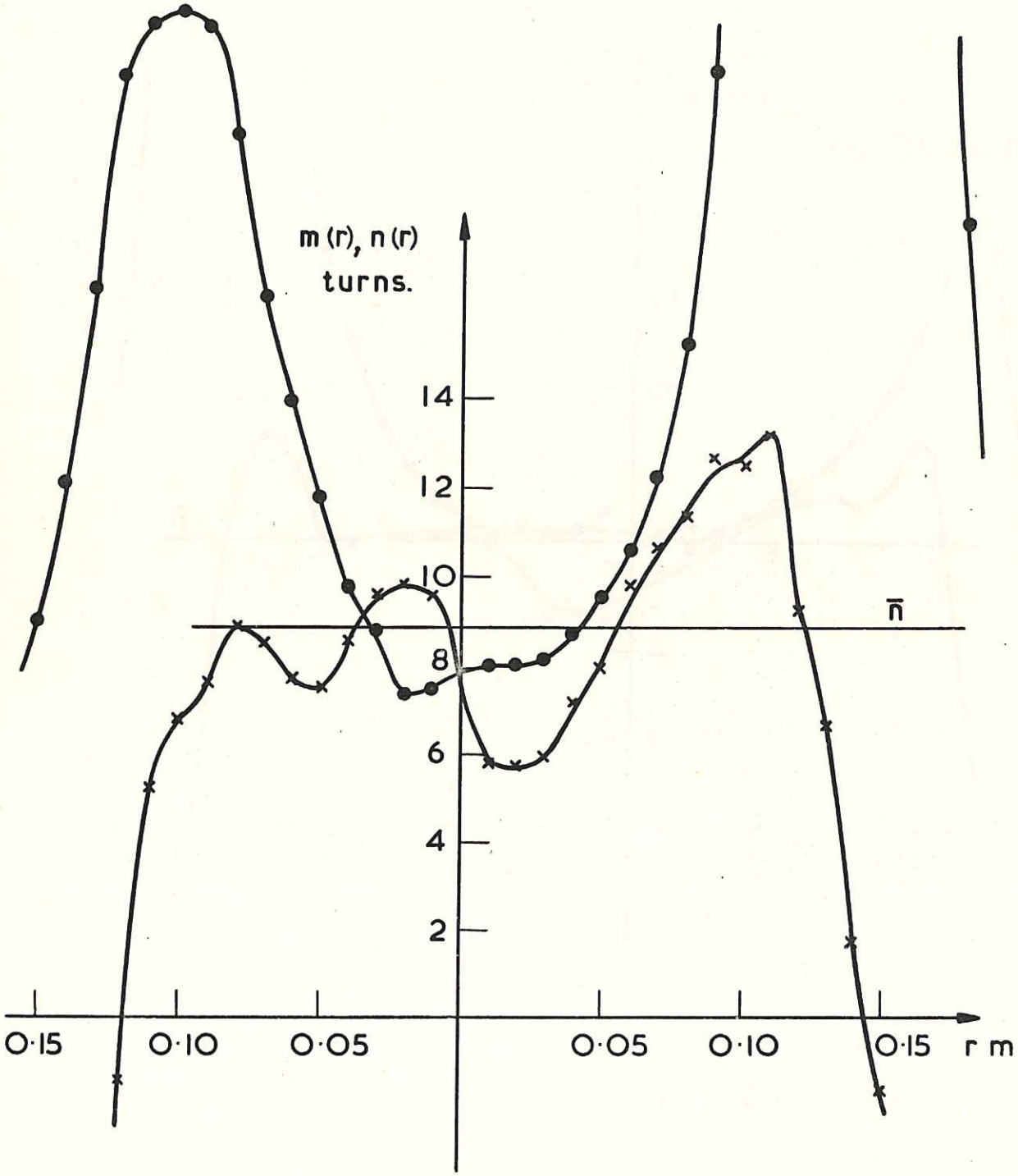

CLM - R7 Fig. 21
m- and n- curves for configuration CIII

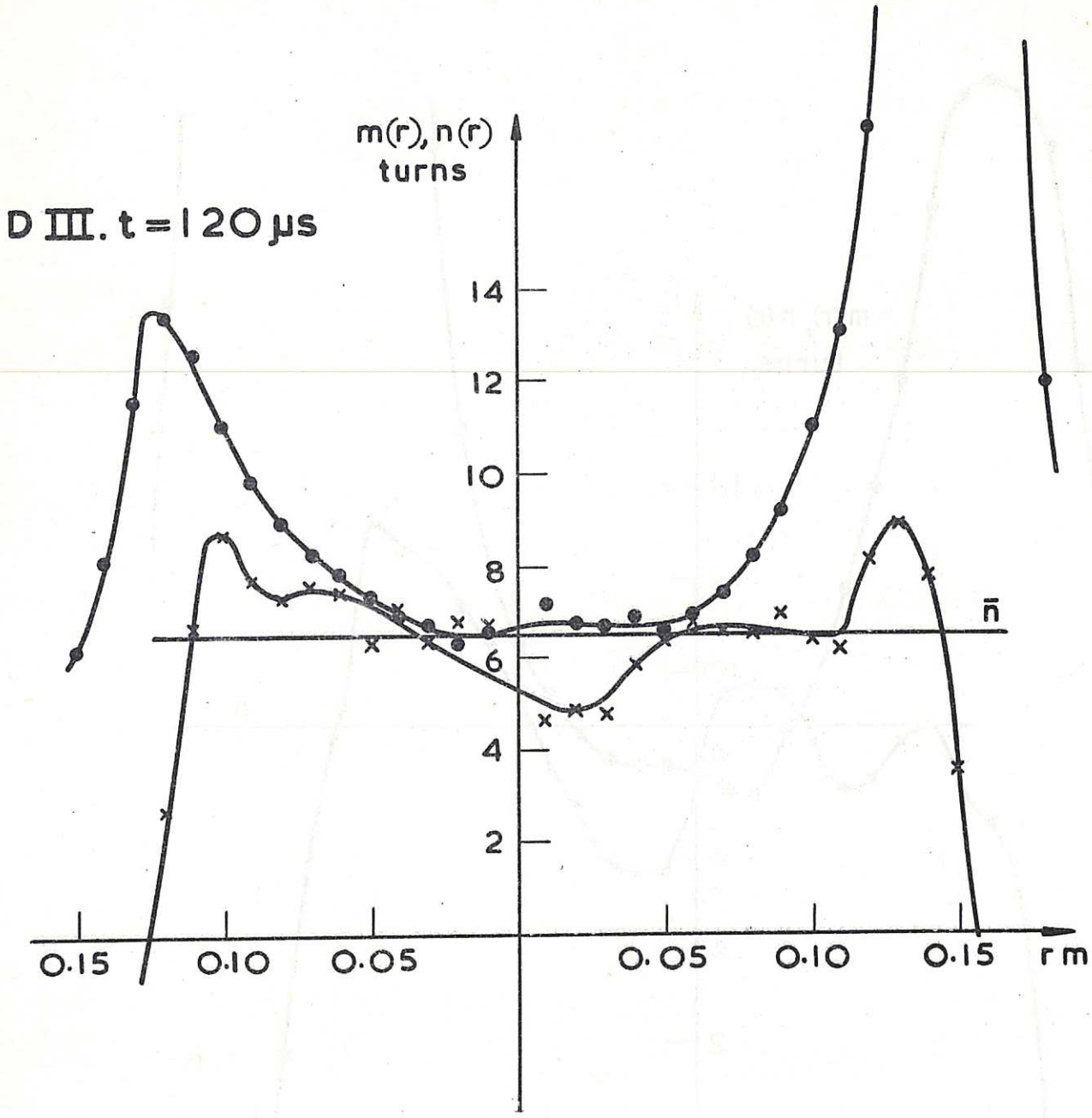

CLM - R7 Fig. 22
m- and n- curves for configuration DIII

Available from
HER MAJESTY'S STATIONERY OFFICE
York House, Kingsway, London W.C. 2
423 Oxford Street, London W. 1
13a Castle Street, Edinburgh 2
109 St. Mary Street, Cardiff
39 King Street, Manchester 2
50 Fairfax Street, Bristol 1
2 Edmund Street, Birmingham 3
80 Chichester Street, Belfast
or through any bookseller.

Printed in England

S. O. Code No. 91 - 3 - 11 - 20